Evaluating the Bond Behavior Between FRP and Grooved Concrete Specimens Using Single Shear Pull Out Test

John Omboko
Marquette University

EVALUATING THE BOND BEHAVIOR BETWEEN FRP AND GROOVED CONCRETE SPECIMENS USING SINGLE SHEAR PULL OUT TEST

by

John Omboko, B.S.

A Thesis submitted to the Faculty of the Graduate School,
Marquette University,
in Partial Fulfillment of the Requirements for
the Degree of Master of Civil Engineering

Milwaukee, Wisconsin

May 2017

ABSTRACT
EVALUATING THE BOND BEHAVIOR BETWEEN FRP AND GROOVED CONCRETE SPECIMENS USING SINGLE SHEAR PULL OUT TEST

John Omboko, B.S.

Marquette University, 2017

Surface preparation affects the bond behavior between Fiber Reinforcing Polymer (FRP) composite material and concrete. In this research, a special type of surface preparation known as grooving, which involves cutting transverse grooves, is conducted on concrete blocks (specimens) that are categorized as either Unfilled (U) or Filled (F). This idea is to ascertain how the grooves affect the strength of FRP-bonded-concrete specimen. These two categories are then benchmarked to control (C) specimens which do not have grooves on them. Category U specimens only have the epoxy applied on the concrete surface while category F specimens have epoxy applied on both the surface and in the grooves. To execute the test, single shear pull out test is conducted under which all the specimens are tested. Results from the test reveal that F specimens are 77% stronger than C specimens. This finding points to the fact that filled specimens possess extra strength due to the presence of epoxy in the grooves, which provide additional contact area and anchorage for the FRP. On the other hand, U specimens have similar strength as C specimens.

Using single shear pull out test, the specimen under the test is designed such that a 25-mm pre-crack condition exist from the front edge of the concrete specimen. This crack mimics the initial debonding and helps to avoid stress concentration at the edge of concrete specimen. Tensile load is then applied on the FRP until failure, and the load, deflection, and strain data recorded using Minnesota Testing System (MTS) and National Instrument (NI) system. Physical appearances of the specimens after failure are observed, which show that failure occurs along the bond length, i.e. debonding failure. A wedge-shaped concrete chunk that breaks at the loading end of the specimen is also observed in most of specimens.

Finally, numerical analysis is performed in order to compare results to experimental results. The analysis employs 3D Finite Element Modeling (FEM) in which all the three categories of the specimens are analyzed. Results from the FEM successfully simulates cracking patterns observed from the experimental tests.

ACKNOWLEDGEMENTS

John Omboko, B.S

Let me start my acknowledgement by expressing my deepest gratitude to my academic advisor, Dr. Wan, for his willingness to work with me. His resolute passion for Civil Engineering research has been such an inspiration and a learning tool for my life endeavors. I salute him for sparing his time and resources to help me succeed in my research. It is because of him that I have been able to expand my engineering horizon and perception. My appreciation also to the Department of Civil, Construction and Environmental Engineering at Marquette University for all the financial assistance.

I would like to also thank Dr. Heinrich and Dr. Foley for their constant support and feedback throughout my Masters program, despite their busy schedules. Much credit to Dr. Heinrich's input and course work that helped me conduct numerical studies for my research using Finite Element Modeling. Special appreciation to Dr. Foley for providing me with more insight throughout my experimental work.

Many thanks to Mr. David Neuman together with his amazing team, Joseph Tschida, Adam Walker, and Mr. Thomas Silman. My experimental work could not have come to life without the team's remarkable performance. I also acknowledge extra help provided by Kaikai Gao, Zhao Wang, Cheng Jiang, and Dr. Xiaohong Zheng.

My humble gratitude to Mr. and Mrs. Jackson and their amazing daughters: Ellie and Julie for what they have done to me including mentoring and exposing me to a new culture. I am truly honored by your support for me to study abroad. Many thanks for staying committed to ensure that I successfully complete my college education. Special

acknowledgment also to Mr. and Mrs. Pastuovic, together with their lovely family: Elizabeth, Colleen, Laura, Christopher, and Catherine. I thank your tireless support and guidance throughout my college studies.

Lastly, I would also like to thank my family in Kenya for believing in me. Thank you so much for your patience and support throughout my studying abroad; you have been a cornerstone in my studies. And to my amazing girlfriend Maureen Ojiambo I can't thank you enough for supporting my pursuit for higher education.

TABLE OF CONTENTS

Acknowledgements i

List of Tables vi

List of Figures vii

1. INTRODUCTION 1

1.1 Background 1

1.2 Research Significance 2

1.3 Research Objective 3

1.4 Organization of the Thesis 4

2. LITERATURE REVIEW 6

2.1 Debonding Behavior and Failure Modes 6

Failure Mode Classification 8

2.2 Bond-Slip Behavior 11

2.3 Concrete-FRP Shear Test Methods 18

2.4 The Role of Concrete Surface Preparation 22

Grooving as a Method of Surface Preparation 23

2.5 Summary of Literature Review 26

3. EXECUTION EXPERIMENTAL WORK 29

3.1 Concrete and FRP Preparation 29

Concrete Specimen Preparation 29

Strengthening Elements 32

Concrete Surface Preparations 33

Water Grinding Process 33

Groove Cutting Process 34

Air Pressure Cleaning, Waxing and Taping Process 36

Preparation of Primer and Adhesive, and the Bonding Process 38

Summary of Surface Preparation Method 40
Strain Gauge Attachment Process 41
3.2 Single Shear Pull Out Test Setup 41
Testing Equipment Setup 42
3.3 Data Acquisition System Setup 44
National Instrument (NI) System Setup and Data Acquisition 45
Linear Displacement Sensor Connection 46
Strain Gauge Connection 48
MTS Configuration into NI System 49
3.4 Observation and Discussion of Experimental Work 51
Control Specimens (C) 51
Specimen CI-C4 52
Specimen C5 53
Unfilled Specimens (U) 55
Specimen U1-U2 55
Specimen U3 56
Specimen U4 57
Specimen U5 59
Specimen U6 60
Filled Specimens (F) 62
Specimen F1 62
Specimen F2 63
Specimen F3 65
Specimen F4 66
Specimen F5 68
Specimen F6 69
3.5 Summary of Experimental Work 71

4. FINITE ELEMENT MODELING (FEM) 74

4.1 Element Selection 74

Solid 65 74

Solid 186 76

4.2 Modeling 77

Material Properties 77

Geometrical Setup 78

4.3 Results and Comparison 80

Stress Variation 80

Crack Behavior 82

Load-Displacement Curves 83

4.4 Summary of FEM 86

5. CONCLUSIONS AND FUTURE WORK 87

5.1 Conclusions 87

5.2 Future Work 88

6. REFERENCES 90

LIST OF TABLES

Table 3.1-1: Compressive and tensile strengths for 28-day concrete

Table 3.1-2: Proportions of concrete mixture

Table 3.1-3: Compressive strength for the 7 specimens used in phase II

Table 3.1-4: Various properties of Strengthening Elements

Table 3.1-5: Concrete, FRP and Groove Dimensions

Table 3.3-1: Properties of LDS

Table 3.3-2: Strain gauge properties

Table 3.5-1: Summary Results of Tested Specimens

Table 4.1-1: Non-Linear Input Properties for modeling SOLID65

Table 4.2-1: Material properties

Table 4.2-2: Concrete Nonlinear Properties

LIST OF FIGURES

Fig. 2.1-1 (a): Mid-Span Debonding. (Teng et al. 2007)

Fig. 2.1-1 (b): End Plate Debonding. (Teng et al. 2007)

Fig. 2.1-2: Fan-shaped anchor for minimizing debonding failure (Francesca et al. 2010)

Fig. 2.1-3: Common debonding failure modes. (Teng et al. 2007)

Fig. 2.1-4: Failure modes under push-pull test (Pham et al. 2006)

Fig. 2.2-1: Fitting experimental results using Popovic's equation (Nakaba et al.2001)

Fig. 2.2-2: Comparison of bond-slip models. Pellegrino et al (2008)

Fig. 2.2-3: Lu et al (2005) bond-slip model

Fig. 2.2-4: A proposed new bond-slip model (Chu et al. 2015)

Fig. 2.2-5: Newton-Raphson iteration flow chart for obtaining parameters in E2.2-6. (Chu et al. 2015)

Fig. 2.3-1: Various bond test methods (Chen et al. 2004)

Fig. 2.3-2: Single shear pull out test idealization. (Yao et al. 2004)

Fig. 2.4-1: Groove cutting as surface preparation (Mostofinejad and Mahmoudabadi 2010)

Fig. 2.4-2: Load-displacement curves for specimens with various surface preparations (Mostofinejad and Mahmoudabadi, 2010)

Fig. 2.4-3: Effects of groove depth on bond strength by Mostofinejad and Hosseni (2013)

Fig. 2.4-4: Bond-slip comparison between 5 and 10 mm wide grooves by Mostofinejad and Hosseni (2013)

Fig. 3.1-1: Forney compression and tension test machine

Fig. 3.1-2: A hand water-grinder and grinded specimens

Fig. 3.1-3: Groove cutting, bond area, and pre-crack condition dimensions

Fig. 3.1-4: Groove and pre-crack condition lines marking

Fig. 3.1-5: Specimens with cut grooves

Fig. 3.1-6: Specimens cleaning using cold water and steel brush

Fig. 3.1-7: Waxed filled (F) and unfilled (U) specimens

Fig. 3.1-8: Taping specimens before application of epoxy

Fig. 3.1-9: Curing of specimens after application of Tyfo® S primer

Fig. 3.1-10: Application of Tyfo® TC Epoxy adhesive

Fig. 3.1-11: Bonding FRP to concrete
Fig. 3.1-12: Proposed strain gauge locations
Fig. 3.2-1: Beam dimensions together with pre-crack condition (Mohammadi, 2014)
Fig. 3.2-2: Concrete half-beam dimensions
Fig. 3.2-3: Single shear pull-out test equipment
Fig. 3.2-4: Single shear pull out test set up
Fig. 3.3-1: Steel plate location on the specimen setup
Fig. 3.3-2: Linear Displacement Sensor mounted on the test specimen
Fig. 3.3-3: Linear Displacement Sensor, LDS
Fig. 3.3-4: Connection of LDS to NI data collection system
Fig. 3.3-5: Configuration of LDS into NI system
Fig. 3.3-6: General Purpose Strain gauge
Fig. 3.3-7: Strain Gauge Connection
Fig. 3.3-8: Strain Gauge Configuration in NI System
Fig. 3.3-9: Configuration of MTS load and displacement to NI
Fig. 3.3-10: (a) Load configuration in the NI system
Fig. 3.3-10: (b) Displacement configuration in the NI system
Fig. 3.4-1: Typical Split Failure for specimens C1-C3
Fig. 3.4-2: Load-displacement plots for specimens C1, C2, and C3
Fig. 3.4-3: Specimen C5: (a) Load-Strain; (b) Strain-Displacement; (c) Load-Displacement (c); and (d) Failure Mode
Fig. 3.4-4: Specimen U1: (a) Load-Strain; (b) Strain-Displacement; (c) Load-Displacement; and (d) Failure Mode
Fig. 3.4-5: Specimen U3: (a) Load-Strain;(b) Strain-Displacement; (c) Load-Displacement; and (d) Failure Model
Fig. 3.4-6: Specimen U4: (a) Load-Strain; (b) Strain-Displacement; (c) Load-Displacement; and (d) Failure Mode
Fig. 3.4-7: Specimen U5: (a) Load-Strain; (b) Strain-Displacement; (c) Load-Displacement; and (d) Failure Mode
Fig. 3.4-8: Specimen U6: Load-Strain; (b) Strain-Displacement; (c) Load-Displacement; and (d) Failure Mode

Fig. 3.4-9: Specimen F1: (a) Load-Strain; (b) Strain-Displacement; (c) Load-Displacement; and (d) Failure Mode
Fig. 3.4-10: Specimen F2: (a) Load-Displacement; and (b) Failure Mode
Fig. 3.4-11: Specimen F3: (a) Load-Strain; (b) Strain-Displacement; (c) Load-Displacement; and (d) Failure Mode
Fig. 3.4-12: Specimen F4: (a) Load-Strain; (b) Strain-Displacement; (c) Load-Displacement; and (d) Failure Mode
Fig. 3.4-13: Specimen F5: (a) Load-Strain; (b) Strain-Displacement; (c) Load-Displacement; and (d) Failure Model
Fig. 3.4-14: Specimen F6: (a) Load-Strain; (b) Strain-Displacement; (c) Load-Displacement; and (d) Failure Mode
Fig. 4.1-1: SOLID 65 Element Type (ANSYS 2016 Element Reference)
Fig. 4.1-2: SOLID 186 Element Type (ANSYS 2016 Element Reference)
Fig. 4.2-1: Geometrical setup for Control, Unfilled, and Filled models
Fig. 4.2-2: Meshed models
Fig. 4.2-3: Load Application – boundary condition and displacement control
Fig. 4.3-1: Nodal stress (MPa) variation in the z-direction for Control (a), Unfilled (b), and Filled (c) models along the direction of load application
Fig. 4.3-2 (a): Crack pattern comparison for control specimen
Fig. 4.3-2 (b): Crack pattern comparison for unfilled specimen
Fig. 4.3-2 (c): Crack pattern comparison for filled specimen
Fig. 4.3-3: Load-displacement for control (a), unfilled (b), and filled (c) specimen

Chapter 1 Introduction

1.1 BACKGROUND

Concrete beams and columns lose their strength because of unexpected increase in load requirements which may have been unaccounted for during the design process, natural hazards such as earthquakes and typhoons, poor maintenance, and steel rebar corrosion due to high chloride agents which are often used as de-icing salts during winter. This has led to the emergence of Fiber Reinforcing Polymer (FRP) composite materials which have gained recognition due to their ability to increase load carrying capacity of the deteriorating concrete members on which they are retrofitted.

While the material is majorly applied on the deteriorating structures, however, FRP can also be used on new structures such as bridge decks and pedestrian bridge systems. When they are incorporated in new structures, repair and maintenance costs are greatly cut down (Sayed-Ahmed et al. 2009).

FRP is made of fibers embedded in resins. Unlike steel, FRP is an anisotropic material whereby its properties vary with direction. Thus, the material is stronger in the direction of the fiber orientation. When the moment capacity of any concrete members is to be improved, FRP is attached on the tensile face to strengthen them in flexure thus increasing the load carrying capacity.

As an alternative construction material, FRP has some major pros over steel and concrete. The material is more preferred because of its high strength-to-weight ratio. The material is easy to apply during repair and rehabilitation as it is very light. The material is

also corrosion resistance and possesses impressive fatigue strength. Minimal time is required when the material is applied externally on the tensile face of concrete members. Although FRP is an excellent strengthening material, ***debonding failure*** is a major setback that the FRP-strengthened members suffer from. This failure is usually brittle and sudden, leading to delamination or cover separation hence the full strength of the material is never utilized.

Such failure, which is initiated from the end of the FRP plate/sheet or at the shear/flexural crack, has led to numerous studies in understanding both the bond and the interface behavior between concrete and FRP. Various failure modes such as, Mode I (interfacial debonding), Mode II (shear-tension failure), Mode III (FRP tensile rupture), Mode IV (cohesion failure), and Mode V (FRP delamination) have also been studied to provide a more comprehensive understanding of the composite action between concrete and FRP (Pham et al. 2006). Additionally, these studies have been conducted through experimental tests such as pull tests, push tests, and beam tests (Yao et al. 2004)

1.2 RESEARCH SIGNIFICANCE

As already pointed out, the major critical downside which affects the strength and capacity of concrete elements with externally bonded FRP is debonding. The current study explores a method whereby transverse grooves are cut on concrete surface before FRP being applied to improve the bond between FRP and concrete, thus postponing debonding failure. While the grooving method has already been conducted by various researchers, in the current study, bond strength will be evaluated using two types of

grooved concrete specimens: unfilled (U) and filled (F). U specimens will lack adhesive epoxy in the grooves while F specimens will have. Furthermore, Finite Element Modeling (FEM) will be conducted to ascertain the stress variation, cracking pattern in each type as well as the load-displacement graphs. The results from experiment and FEM analysis will help provide an entry into the intricacies surrounding FRP-concrete bond. It will also help engineers improve their understanding of the bond behavior between FRP and concrete that is aimed at enhancing the load capacity of FRP retrofitted concrete structures.

1.3 RESEARCH OBJECTIVE

The major objective of the current study is to evaluate the bond behavior between carbon FRP (CFRP) plate and transversely grooved concrete blocks using single shear pull-out test. Further analysis of the experiment is done using FEM.

The experimental data results are geared towards helping understand the load-strain relationship, failure modes and the impact of both epoxy-filled grooves and unfilled grooves. On the other hand, FEM helps to understand both the linear and non-linear phases of load-displacement curves as well as failure mechanism/mode for FRP-concrete bond including the cracking pattern.

1.4 ORGANIZATION OF THE THESIS

With the current study aimed at evaluating the bond behavior between FRP and transversely grooved concrete blocks using both experimental and numerical work, the steps in achieving this goal are broken down as follows:

A brief background and general information on FRP are presented in *Chapter 1: Introduction*. This chapter also presents advantages and disadvantages of FRP as well as the concept of debonding. Lastly the chapter explains research significance and objectives.

Chapter 2: Literature Review, presents experimental findings and tests conducted by various studies. These studies touch on four major areas of interest: debonding behavior and failure modes; bond-slip behavior; concrete-FRP shear test methods; and the role of concrete surface preparation. A detailed explanation backed by references is provided for all the four areas. Finally, this chapter is completed by provide a summary takeaway.

Chapter 3: Execution of Experimental Work, jumps into all the experimental work conducted including test systems set up, data collection and analysis as well as discussion of the results obtained from the tests. Finally, this chapter provides takeaways obtained from executing experimental work.

Analytical work using finite element analysis package, ANSYS 17.1, is presented in *Chapter 4: Finite Element Modeling (FEM)*. In this chapter, replica models for control, unfilled and filled models are created and analyzed using appropriate element selection and meshing. Results obtained are then compared to experimental results and conclusion drawn.

Before wrapping up the study, general conclusions are provided. These conclusions provide major learning lessons obtained from conducting the research. Not only are conclusions provided but also recommendations for future work. These recommendations try to provide suggestions on to improve the results obtained by minimizing the errors that were observed. All these are covered in *Chapter 5: Conclusions and Future Work*.

Chapter 2 Literature Review

2.1 DEBONDING BEHAVIOR AND FAILURE MODES

Debonding is a premature failure type where the FRP material peels off the concrete surface because of increased stress in the concrete-FRP bond interface. Such failure inhibits full FRP material strength and therefore the flexural capacity of the strengthened member is compromised. Various failure modes have been observed to occur when this type of failure happens. They, however, have one thing in common: once they occur, FRP is normally seen with small chunks of concrete on its contact surface. It should be noted that failure modes relate to how the FRP debonds from concrete substrate.

Several studies have classified premature debonding into two categories: ***end plate debonding*** and ***mid-span debonding***. End debonding occurs at the end of FRP anchorage length while mid-span debonding occurs in the middle of the anchorage length due to intermediate cracks which are initiated by high bending moment in the middle of the strengthened member. Figs. 2.1-1 (a) and (b) show both mid-span and end plate debonding. Major observable features associated with premature debonding include crushing of concrete in compression before yielding of reinforcement, yielding of steel in tension followed by rupture of FRP laminate, concrete cover delamination/peel off, and FRP debonding from concrete substrate. While the first two failure modes are common, the third type normally happens when a thin (<1.0 mm) FRP is bonded on an uneven concrete surface (Swamy et al. 1999). Lu et al. (2005), together with other studies have

established that debonding of FRP from concrete substrate happens between 2-5 mm of concrete layer adjacent to adhesive layer.

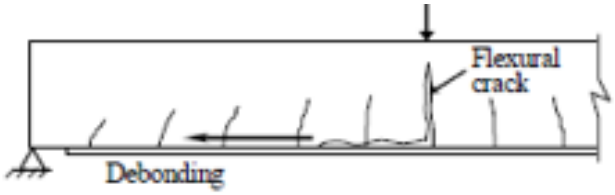

Fig. 2.1-1 (a): *Mid-Span Debonding. (Teng et al. 2007)*

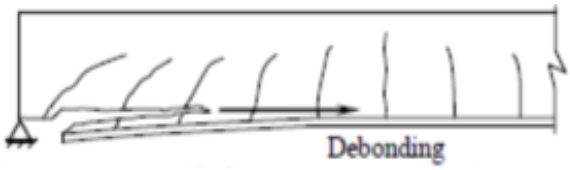

Fig. 2.1-1 (b): *End Plate Debonding. (Teng et al. 2007)*

For externally strengthened members, it has been observed that debonding happens near the FRP ends due to transfer of stress from concrete to FRP. Not only does this lead to FRP debonding, but also causes diagonal cracks in concrete that help accelerate the debonding process. Studies have shown that when sufficient anchoring system is put in place, then this kind of debonding can be minimized or even delayed. Francesca et al (2010), evaluating the bond strength in concrete with externally reinforced CFRP and anchoring devices, found that by using fan-shaped anchors as that shown in Fig. 2.1-2, more anchoring load capacity is realized for shear. It is also seen that debonding depends on the both physical and mechanical properties of concrete, FRP, and the adhesive epoxy (Mazzotti et al. 2007).

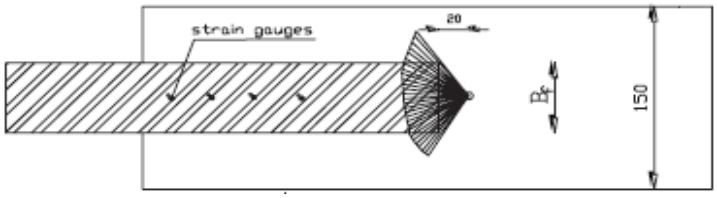

Fig. 2.1-2: *Fan-shaped anchor for minimizing debonding failure (Francesca et al. 2010)*

Failure Mode Classifications

FRP debonds from concrete surface in several ways because of its brittle nature. This causes sudden failure due to stress concentration at various locations along the bond length. Some of the notable failure modes include the following.

Plate End (PE) Debonding: This type of debonding is caused by large normal and shear stresses that occur at the end of the plate/sheet, and it propagates through concrete cover up to the level of internal reinforcement. Such type of failure is normally witnessed in concrete beams that have very slender FRP materials than the beam section (Teng et al. 2007). Even though this type of debonding affects the strength of retrofitted member, however, it can be curbed by using transverse reinforcement such as U-FRP stirrups, ensuring that the FRP end extends into the uncracked region of the member or by using mechanical anchorages.

Intermediate Crack-Induced (IC) Debonding: This mode is usually visible at the shear span of the member and propagates towards the end of the beam, i.e. direction of decreasing moment, leading to concentration of large local strains. After cracking, released tensile stress causes high interfacial stresses between FRP and concrete. This type of debonding can initiate multiple cracks across the shear span of the member. It is the most commonly observed mode of failure; it is also known as Mode 1 (Pham et al. 2006 and Teng et al. 2007). However, continuous transverse reinforcement can help reduce this type of debonding.

Axial Intermediate Crack Debonding: This type of debonding refers to direct pull tests where there is no curvature in concrete and the FRP is in tension. This mode is also known as Mode 3 – tensile rupture mode, and is usually common for FRPs with very small cross sections (Yao et al. 2004; Pham et al. 2006).

Critical Diagonal Crack-Induced (CDC) Debonding: Very identical to crack-induced debonding even though it is related to single critical shear crack. This debonding is associated with members strengthened in flexure and with limited shear reinforcement. Diagonal cracks which intersects the FRP are observed to occur leading to failure (Yao et al. 2004)

Interfacial Shear-Induced Debonding: Also called Mode 2 – tensile failure mode. In this mode, the main crack propagates from the FRP end into the concrete substrates, as shown in Fig. 2.1-3. While it is not common, this type of debonding can govern the behavior of FRP bonded to prestressed members in which cracking is suppressed. It is also visible in cases where very thick FRP is used to regulate deflection for service loads (Yao et al. 2004). Other studies have shown that this type of failure mode happens when there is a small chunk of concrete close to the interface that is subjected to very high shear stress (Pham et al. 2006 and Mazzotti et al. 2007). Fig 2.1-3 shows some of the common failure modes which occur on concrete members bonded with FRP laminates.

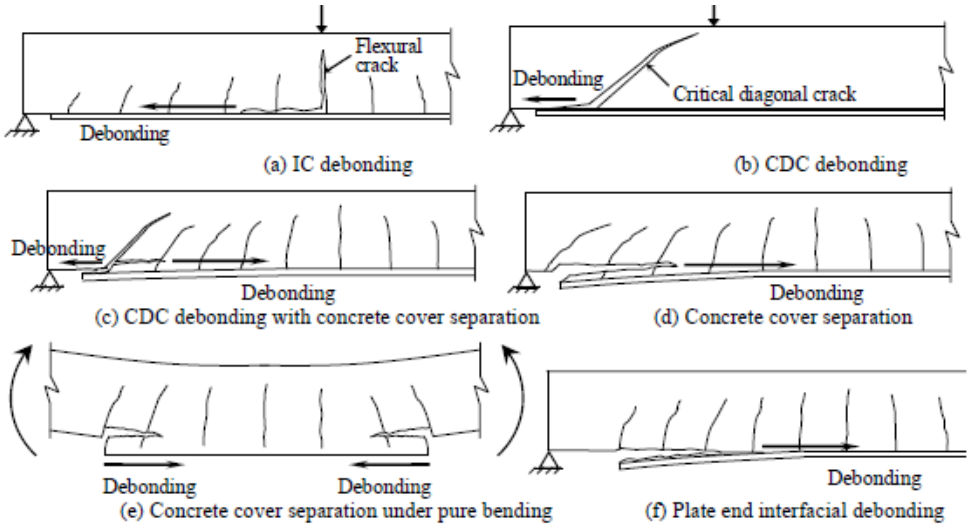

Fig. 2.1-3: *Common debonding failure modes. (Teng et al. 2007)*

Other notable failure modes are: *concrete cover separation*, where cracks along the tensile face of concrete are propagated. Cracks are initiated at the end of the plate and as loading continues, cracks continue to widen leading to cover separation; *peeling* failure mode occurs once uniformly spaced cracks develop due to shear and normal stress concentration at the end of the FRP plate/sheet. As loading continues, many cracks develop that cause concrete segments formation between two adjacent cracks, thus leading to peeling of FRP. This mode is also called Mode 5 – delamination mode. Fig. 2.1-4 shows other notable failure modes which have been reported under the push-pull test (Yao et al. 2004; Pham et al. 2006 and Teng et al. 2007)

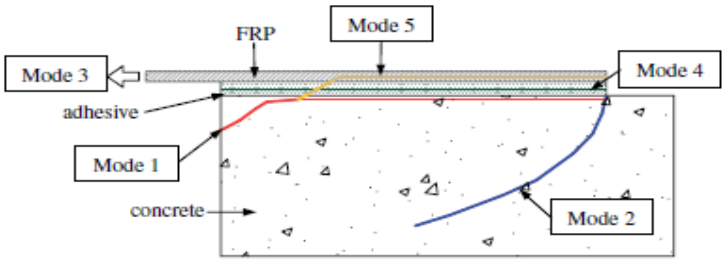

Fig. 2.1-4: *Failure modes under push-pull test (Pham et al. 2006)*

Even though debonding failure is still a major problem for concrete members bonded with FRP, several recent studies have provided some solutions on how to minimize this type of failure. For instance, FRP sheets can be wrapped around the concrete web over the longitudinal FRP sheet. Swamy et al (1995) have noted that such failures can also be minimized by ensuring that FRP width-to-thickness ratio to be not less than 50. Additionally, longitudinal FRP plates/strips can be firmly anchored on the tensile face of the member by using bonded angle plates/strips or transverse FRP wraps.

2.2 BOND-SLIP BEHAVIOR

Retrofitting and rehabilitating deteriorating structures using FRP helps to safeguard them against failures due to disasters like earthquakes; poor construction and maintenance; and fatigue. While retrofitting method helps to improve the strength and load capacity of structures, however, studies show that the strength of FRP plate is rarely fully utilized due to premature debonding when it is bonded on the tensile face of concrete. This failure is usually very brittle and hard to predict. Among the many failures encountered during tests include, interfacial debonding, cover/plate separation, plate-end interfacial debonding, intermediate crack induced interfacial debonding, and critical diagonal crack induced interfacial debonding.

It is then of critical concern to understand the bond behavior between concrete and FRP in order to generate models that could help engineers design against such sudden failures. To achieve this, experimental tests, usually shear or beam tests, are conducted and the data obtained used to generate a bond-slip curve. The curve consists of

an ascending branch followed by a descending branch. In many instances, the two branches are usually exponential although bilinear curves have been generated as well (Lu et al. 2005 and Pellegrini et al. 2008). One of the major importance of generating a bond-slip curve is to help accurately determine the interfacial fracture energy, G_f, which affects the ultimate strength of the FRP-concrete bond. The interfacial fracture energy is computed as the area under the bond-slip curve (Pellegrino et al. 2008).

Following the behavior for a typical bond-slip curve – ascending part followed by a descending part – many researchers have used the curve to generate mathematical equations which help to compute interfacial fracture energy. Some of the mathematical models which are already in use include those of Lu et al (2005), Dai and Ueda (2003), Monti et al (2003), Nabaka et al (2001), and Rostasy and Neubaure (1999). It should be noted, however, that these models are based on theoretical assumptions (Pellegrino et al. 2008). Moreover, the models have three parameters in common which are associated with bond slip curve: ultimate slip, s_{ult}, where the bond stress falls to zero and relates to local debonding of FRP from concrete, the maximum shear bond stress, τ_{max} and slip at peak bond strength, s_{peak} (Pellegrino et al. 2008).

Nakaba et al (2001) found that effective bond length was the distance between two points that corresponded to 10% of the maximum bond stress, following Popovic's equation. The study also revealed that the maximum load increased with increase in FRP stiffness. However, bond interface thickness did not have any effect on the maximum load, which conflicts with some other studies. Additionally, it was found that concrete compressive strength had influence on the local bond stress in that as compressive

strength increased, so did the local bond stress. Fig. 2.2-1 shows local bond stress-slip relationship fitted to Popovic's equation (E2.2-1).

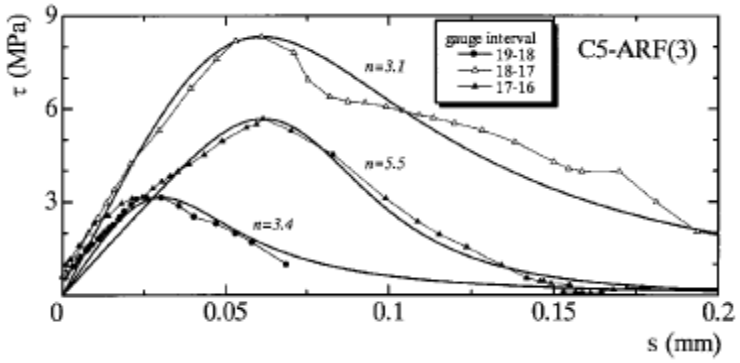

Fig. 2.2-1: *Fitting experimental results using Popovic's equation (Nakaba et al.2001)*

$$\frac{\tau_b}{\tau_{b,max}} = \frac{s}{s_{max}} \cdot \frac{n}{(n-1) + \left(\frac{s}{s_{max}}\right)^n} \qquad (\mathbf{E2.2-1})$$

Where $\tau_{b,max}$ is the maximum local bond stress; s_{max} is the maximum slip at $\tau_{b,max}$ and n is a constant

In the above equation, $\tau_{b,max}$ and s_{max} are directly obtained from the experimental τ_b versus s relationship, while the value of n is obtained following least square method using normalized τ_b versus s relationship. Studies have further established that fracture energy, which is the area under the bond-slip curve, depends largely on the properties of concrete used. It is worth noting that the FRP-concrete bond strength is directly proportional to the square root of fracture energy, G_f irrespective of the shape of the stress bond-slip curve (Lu et al. 2003 and Pellegrino et al. 2008)

Pellegrino et al (2008), conducting double shear and bending tests on twenty concrete specimens under different parameters such as different FRP types and rigidities, established a new bond-slip model shown in equation E2.2-2 below.

$$G_f = \frac{\tau_{max} \cdot s_{peak}}{1575} + \frac{\tau_{max}}{\left({s_{peak}}^{\alpha} - {s_{ult}}^{\alpha}\right) \cdot (\alpha + 1)} \left({s_{peak}}^{\alpha} \cdot s_{peak} - {s_{peak}}^{\alpha+1}\right) \qquad (\mathbf{E2.2-2})$$

where,

$$\alpha = -\frac{13162}{\left(n_f E_f t_f\right)^{0.187}}$$

and $n_f E_f t_f$ is the axial rigidity (GPa.mm).

Fig. 2.2-2 shows bond-slip curves comparison between experimental, existing analytical model and the new model proposed by Pellegrino et al (2008). As can be seen, the new proposed model provides a much better estimation as it captures an ultimate shear stress of about 15 MPa.

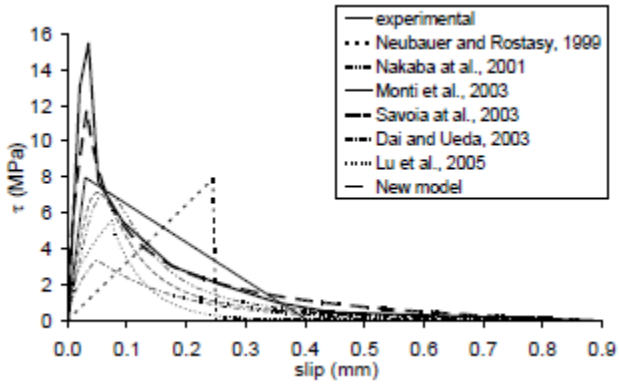

Fig. 2.2-2: *Comparison of bond-slip models. Pellegrino et al (2008)*

Obaidat (2003) acknowledges that debonding due to stress concentration at various locations in both concrete and FRP inhibits fully utilization of composite strength action and recommends a bond-slip model that does not rely solely on geometric

parameters. She also notes that while the existing bond-slip models help improve the performance of FRP on concrete, however, very few studies have been conducted to assess the performance of interfacial load transfer between concrete and FRP. To model the interface, she uses cohesive zone model together with Lu et al's bond slip model shown in Fig. 2.2-3.

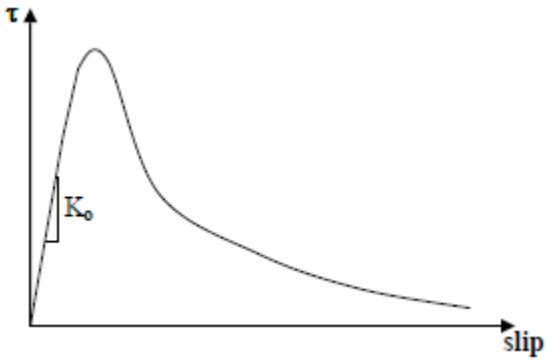

Fig. 2.2-3: *Lu et al (2005) bond-slip model*

K_o in Fig 2.2-3 is given as;

$$K_o = \left(\frac{G_i G_c}{G_c t_i + G_i t_c}\right) \qquad (\mathbf{E2.2-3})$$

where t_i and t_c are the adhesive and concrete thickness respectively and G_i and G_c are shear modulus of adhesive and concrete respectively. Maximum shear stress and fracture energy are obtained using equations E2.2-4 and E2.2-5 respectively.

$$\tau_{max} = 1.5\beta_w f_{ct} \qquad (\mathbf{E2.2-4})$$

$$G_f = 0.308(\beta_w)^2\sqrt{f_{ct}} \qquad (\mathbf{E2.2-5})$$

where $\beta_w = \sqrt{\frac{\left(2.25-\frac{b_f}{b_c}\right)}{\left(1.25+\frac{b_f}{b_c}\right)}}$

Results from the test revealed that fracture energy increased with increasing maximum load, and that interfacial stiffness was dependent on shear modulus and adhesive thickness between concrete and FRP. This stiffness was also related to load transfer between concrete and FRP. Using a procedure of inverse analysis, Chu et al. (2015) modified Yuan et al. (2001) bond-slip model and proposed a new model as shown in Fig. 2.2-4, which is made of two parts: the bilinear ascending part followed by a descending exponential part.

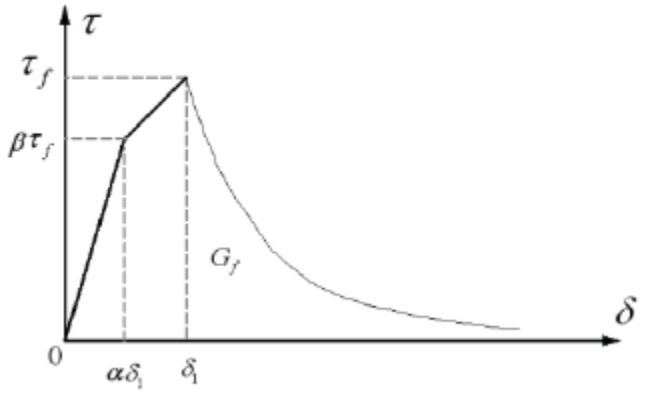

Fig. 2.2-4: *A proposed new bond-slip model (Chu et al. 2015)*

As seen in Fig. 2.2-4, the first separating point on the ascending branch is at ($\alpha\delta_1$, $\beta\tau_f$). This point indicates a slope transition of the bond-slip correlation on the linear-elastic behavior. Such observation is based on studies done by Ueda et al (2003), Savioa et al (2003), and Nakaba et al (2001) (Chu et al. 2015). The above curve is useful since it helps to evaluate the interfacial shear stress in concrete-FRP bond using the following generated equation:

$$f(\delta) = \begin{cases} \beta\dfrac{\tau_f}{\alpha\delta_1}, & 0 \le \delta < \alpha\delta_1 \\ \dfrac{\tau_f}{1-\alpha}\left[\dfrac{(1-\beta)\delta}{\delta_1} + (\beta-\alpha)\right], & \alpha\delta_1 \le \delta \le \delta_1 \\ \tau_f e^{\frac{-\tau_f}{k}(\delta-\delta_1)}, & \delta_1 \le \delta \end{cases} \qquad (\mathbf{E2.2-6})$$

where, δ_1 is the bond slip at the maximum bond shear stress and τ_f is the maximum shear stress. The five unknown parameters, τ_f, bond strength; δ_1, slip at bond strength; k, interfacial fracture energy; α, and β are determined following finite element analysis using single pull out shear test model, with the help of Newton-Raphson iteration method shown in Fig. 2.2-5 (Chu et al. 2015).

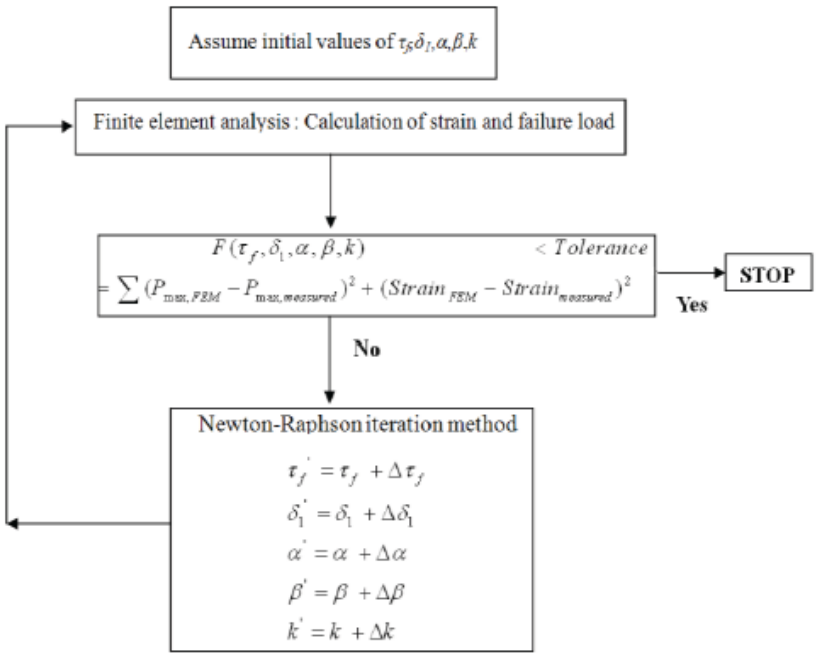

Fig. 2.2-5: *Newton-Raphson iteration flow chart for obtaining parameters in E2.2-6. (Chu et al. 2015)*

The first three unknowns, τ_f, δ_1, k are directly related to concrete compressive strength and indirectly related to the bond width; however, it is determined that the bond length does not affect the three parameters (Chu et al. 2015). Following the studies conducted by Ueda et al (2003), Savioa et al (2003) and Nakaba et al (2001), the two remaining parameters, α and β are found to be 0.5 and 0.7 respectively. Furthermore, these two parameters help to determine the separating point in the bilinear elastic ascending part of the bond-slip curve.

2.3 CONCRETE-FRP SHEAR TEST METHODS

Shear test is the most common used type of test for evaluating the bond strength between concrete and FRP as well as the bond slip behavior. Because of its simplicity and effectiveness, this test is preferred to compressive or tensile test.

For single shear pull-out test, a concrete block is kept in place with support block bearing against the concrete surface near the loaded end while the rotation of the concrete block is resisted by a steel clamp. Pham et al (2006) notes that the main advantage of this method is that experimental material usage can be reduced. Apart from single pullout test, other notable shear tests include, single shear push test, double shear pull test, double shear push test. Beam test method has also been used to understand the physical and mechanical properties of the adhesive interface in the concrete-FRP bond. Fig. 2.3-1 shows some of the common bond test methods. Chen et al (2004) refers single shear pull test as far end support (FES) single shear test; single shear push test as near end support (NES) single shear test; double shear pull test as far end support (FES) double shear test; and double shear push test as near end support (NES) double shear support. In all these tests, FRP plate is always pulled away from the concrete substrate using applied tensile force, hence the tests are sometimes collectively referred to as pull tests.

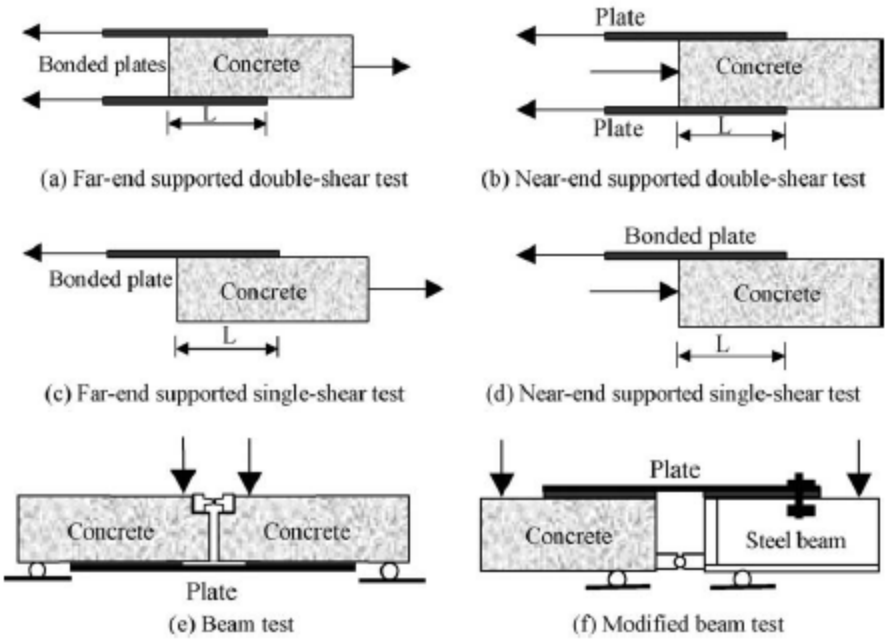

Fig. 2.3-1: *Various bond test methods (Chen et al. 2004)*

To test the effectiveness of single shear pull-out test, Chen et al (2004) conducted studies on 72 specimens to evaluate how various parameters – bond length, width ratio between FRP and concrete block, height of concrete free edge, and offset of load position – affected the bond strength between concrete and FRP. It was found that the first two parameters affected concrete-FRP bond strength, while the height of concrete free edge affected stress distribution in the specimen significantly.

Mazzotti et al (2007), conducting tests using single push-pull test observed that there was no significant effect of FRP width on delamination force per unit width. It was also found that increasing FRP plate width decreased the peak shear stress more than predicted by already available formulas. Similarly, due to its simplicity, Yao et al (2004) conducted single shear pull-out test to understand the shear crack-induced failures as well as flexural shear crack-induced debonding failure. In the experiment, it was recorded that the height of the free edge of concrete impacts the bond strength. When the top of support

is very close to the FRP plate, local stress near the loaded end is increased. Such increased local stress leads to early debonding due to reduced bond strength.

To evaluate factors such as bond length, bond width, and concrete strength, several specimens were tested by Chu et al. (2004) using pull-out test method. Common features were seen in the tested specimens: cracks that propagated from the edge of concrete due to continued loading; failure of FRP due to ultimate loading; and longitudinal splitting of some FRP plates after failure, with epoxy seen attached on some. The test further found that increasing bond length, bond width and concrete strength led to delayed failure as specimens picked up more load. Under the test, results showed that concrete strength did not greatly affect the load capacity of the composite; only a 10 % increase was recorded.

Fig 2.3-2 shows idealization of single shear pull-out test for evaluating various parameters such as bond length, L_{frp}, height of concrete free edge, h_c and the offset of load position, δ as conducted by Yao et al (2004).

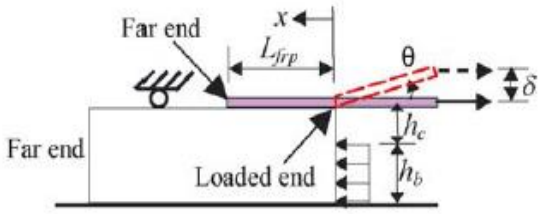

Fig. 2.3-2: *Single shear pull out test idealization. (Yao et al. 2004)*

Pull-out tests have further shown that a measurable bond length exists beyond which no further increase in the transferred load could be obtained (Bizindavyi et al. 1999). Other than push/pull and beam tests, *mixed-mode bond* test has also been used. This method is more representative of the interface bond behavior for FRP material retrofitted on concrete structures. The method is composed of variable angle peel test,

beam type and slab type dowel tests, single contoured cantilever beam test, the double cantilever beam test, and the modified double cantilever beam test (Wan et al. 2006). Unlike push/pull and beam tests, mixed-mode beam tests are relatively hard to conduct and interpret the test results.

2.4 THE ROLE OF CONCRETE SURFACE PREPARATION

The goal of concrete surface preparation is to improve the bond between FRP and concrete in order to delay the debonding failure and to ultimately increase the composite strength. However, as will be discussed in the paragraphs to follow, different surface preparation yields different results. Generally, the procedure is conducted by scraping off few millimeters of weak concrete surface on the specimen to be tested so as to expose the strong aggregate layer. Mechanical grinders, sand blasting, grit blasting, air pressure jets, and water jets are commonly used methods to remove the weak layer that might otherwise impede the bond strength.

For a quality bond to be realized between concrete and FRP, surface preparation workmanship needs to be good. Surface preparation impacts bond quality since it ensures that the surface on which the FRP is bonded on is free of any loose particles and dust. For single shear pull out test, surface preparation is crucial as it helps to expose small to medium-sized aggregate that provide a good bond. While this is the case, however, it is worth noting that it is laborious to achieve a uniformly flat concrete surface using the available surface preparation methods that can guarantee a uniform epoxy thickness (Sayed-Ahmed et al. 2009). Thus “a uniform thickness” of epoxy is often assumed when

FRP is slightly pressed hard against concrete during the bonding process and allowing the excess epoxy to be removed from the sides.

Toutanji and Ortiz (2001) used two methods to study how the effects of surface preparation affects the bond strength between FRP and concrete. The methods were cleaning concrete using an ordinary sander that was to help get rid of a thin layer of weak concrete and using water jet. After surface preparation and application of epoxy, it was found that by using water jet as a method of specimen surface preparation, the FRP-concrete bond strength was increased significantly as the specimens recorded higher failure loads. This increase was 50% higher than those specimens prepared using ordinary sander.

With good quality surface preparation, greater interfacial consistency and continuity between concrete and FRP plate/sheet is assured. This in turn leads to higher ultimate failure load due to delayed debonding. Not only does a cleaned surface influence the bond results but also concrete strength as well as the lining layer on which the epoxy is applied (Mostofinejad and Mahmoudabadi, 2010). With proper cleaning, there is a desirable transfer of shear stress that exist between concrete and FRP. Previous studies have revealed that with proper surface preparation, bond strength increases from 3-10%, especially when high pressure waterjet is used. Furthermore, Mostofinejad and Mahmoudabadi (2010), cutting various grooves in concrete as a form of surface preparation, noted that transverse grooves led to increased epoxy contact area thus increasing the bond strength by 10% compared to specimens without grooves.

Grooving as a Method of Surface Preparation

Mostofinejad and Hosseni (2013) and Mostofinejad and Mahmoudabadi (2010) devised a new method of surface preparation which is aimed at improving the bond behavior between concrete and FRP. The method includes cutting grooves – transverse, diagonal and longitudinal – on the concrete substrate as can be seen in Fig. 2.4-1. So, apart from the normal surface preparations, the current study will also incorporate this new method by having transverse grooves on concrete substrate which were selected since they provide more anchorage to the applied load in addition to providing extra bond contact area.

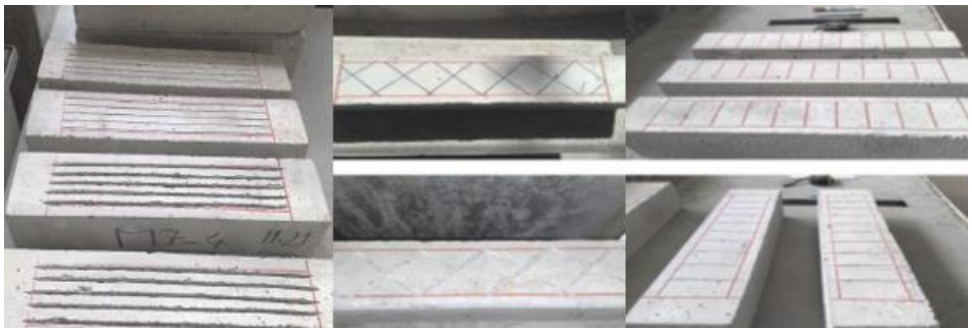

Fig. 2.4-1: *Groove cutting as surface preparation (Mostofinejad and Mahmoudabadi 2010)*

It is observed that by cutting grooves on the concrete surface, a strong contact is created between FRP and concrete which increases the bond strength due to delayed debonding during loading. It is further noted that there is a load increase of 10%, 15% and 27% for transverse, diagonal and longitudinal grooves respectively. While the three groove types provide additional bond contact area, however, longitudinal grooves recorded much higher load capacity since the added groove contact area is parallel to the stress in the bond interface (Mostofinejad and Mahmoudabadi 2010). Fig. 2.4-2 shows

variation of load against displacement for specimens with various surface preparation conditions as reported by Mostofinejad and Mahmoudabadi (2010).

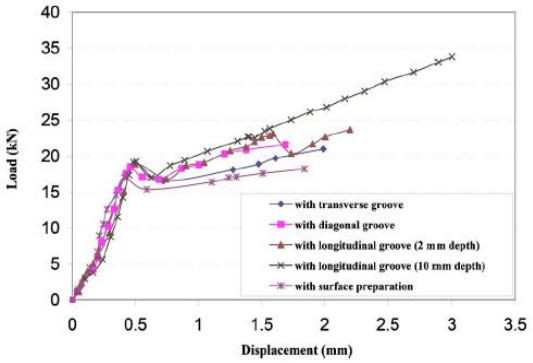

Fig. 2.4-2: *Load-displacement curves for specimens with various surface preparations (Mostofinejad and Mahmoudabadi, 2010)*

Fig. 2.4-2 shows that for specimens with longitudinal grooves, increasing groove depth – from 2 mm to 10 mm – increases load capacity up to 35 kN. This then indicates that by increasing groove depth, bond contact area is increased which in turn delays debonding hence increasing load capacity. Furthermore, the plots show that transverse, longitudinal and diagonal grooves increase contact area that results in higher rupture loading capacity (Mostofinejad and Mahmoudabadi 2010)

All in all, it can be pointed out that, while normal surface preparation which involves removing the deteriorated concrete surface layer increases the bond strength between FRP and concrete, however, addition of grooves on the surface further increases the bond strength. This is the case since grooves – transverse, diagonal or longitudinal – provide additional contact area for the bond between concrete and FRP.

Using accurate image-based deformation measurement technique called Particle Image Velocimetry (PIV), Mostofinejad and Hosseni (2013) studied several specimens to evaluate the effects of externally bonded reinforcement on grooves (EBROG) and found that the method, as a form of surface preparation, increased the ultimate load up to 28%

over the normal surface preparation methods. Not only did the specimens with grooves record a high load but also, their failure was debonding in concrete: CFRP debonded from concrete with a thin layer of concrete attached on it. Fig 2.4-3 shows variation of load against end slip for specimens with 5 mm groove depths as recorded by Mostofinejad and Hosseni (2013).

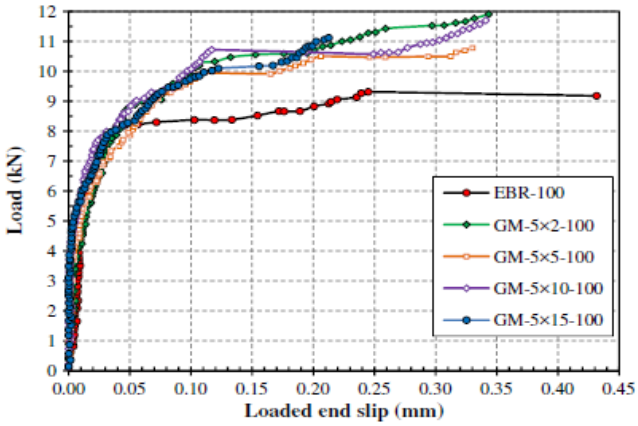

Fig. 2.4-3: *Effects of groove depth on bond strength by Mostofinejad and Hosseni (2013)*

Mostofinejad and Hosseni (2013) further observed from the load-slip behavior analysis using PIV that wider grooves provide stronger bond strength. The technique also indicated that EBROG method is stronger than conventional surface preparation methods as larger strain values were recorded. Thus, it was concluded that groove width also played a key role in the bond strength between FRP and concrete. Fig. 2.4-4 compares bond strength for specimens with groove width of 5 mm and 10 mm as recorded by Mostofinejad and Hosseni (2013).

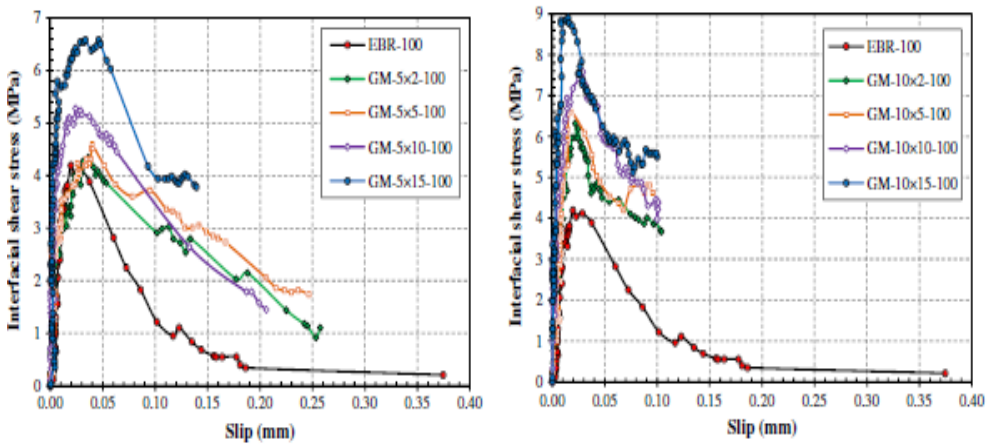

Fig. 2.4-4: *Bond-slip comparison between 5 and 10 mm wide grooves by Mostofinejad and Hosseni (2013)*

2.5 SUMMARY OF LITERATURE REVIEW

The goal of this chapter, **Literature Review**, has been to explore various studies around concrete-FRP bond. Broken into four major categories, debonding behavior and failure modes; bond-slip behavior; FRP-concrete bond test methods; and the role of concrete surface preparation, the chapter has detailed a wide range of studies together with their findings on how to develop and improve the bond strength between concrete and FRP. The highlights of the chapter are listed below:

- Debonding failure is a major setback affecting concrete structures retrofitted with FRP. This failure is often premature, sudden and brittle. Full flexural capacity of the FRP-concrete composite is usually inhibited because of this failure.
- Small concrete chunks are always visible on FRP after debonding failure.
- Two major debonding types are, end-plate debonding and mid-span debonding. The former occurs at the end of the anchorage length due to high shear and

normal stress concentration while the latter occurs due to intermediate cracks initiated by high bending moments at the mid span of the member.

- Debonding can be classified in distinctive failure modes such as; plate end (PE) debonding; intermediate crack induced (IC) debonding; axial intermediate crack debonding; critical diagonal crack induced (CDC) debonding; and interfacial shear-induced debonding. These are the most notable failure modes as observed from various experiments. Concrete cover separation and peeling failure modes have also been reported in some tests.
- Wrapping FRP sheets around the web of the concrete member, ensuring that FRP width-to-thickness ratio is not less than 50 as well as longitudinal FRP anchored on the tensile face of the retrofitted member have been some of the solutions shown to minimize some of debonding failure modes.
- By generating bond-slip curves from tests and modelling mathematical equations, it becomes easy to understand the bond behavior between FRP and concrete. The curve is made of both ascending and descending parts. The area under the curve can be used to compute fracture energy.
- Many test methods have been used to assess various factors affecting the FRP-concrete composite. Such methods include, single shear pull out test, single shear push test, double shear pull test, double shear push test, and beam test. The first four methods are collectively known as pull tests since FRP is always pulled away from the concrete substrate.
- Perhaps one of the most important factor which governs the bond strength between FRP-concrete bond is the quality of surface preparation. Surface

preparation methods like mechanical grinders, sand blasting, grit blasting as well as water and air pressure jets have been used with the goal to improve the bond strength between FRP and concrete.

- Recent studies have proposed grooving as a form of surface preparation. Specimens with transverse grooves – grooves that run across the beam length – are tested in the experimental program and analyzed using finite element model.

Chapter 3 Execution of Experimental Work

This chapter discuses experimental work, detailing the entire process from concrete blocks preparation to summary of results obtained. Preparation of concrete blocks follows the established standards by ASTM C192/192M-06 while FRP preparation follows manufacturer's standard procedure. Prior to testing the specimens, surface preparations (including groove cutting) are performed to ensure that the weak layer of concrete is removed. Next, the chapter discusses the test method: single shear pull out test, as well as data collecting systems, which include Minnesota Testing Systems (MTS) and National Instruments (NI) system. Observations and discussions of the experimental work are detailed for all the tested specimens. Finally, a summary of the chapter is provided highlighting major findings.

3.1 CONCRETE AND FRP PREPARATION

Concrete Specimens Preparation

All the concrete blocks used in this study were prepared in the Engineering Materials and Structural Testing Laboratory (EMSTL) at Marquette University Opus College of Engineering. A total of 15 concrete blocks were available for the test that was conducted in two phases – phase I and II. Undamaged concrete blocks from phase I were used in phase II. In the first phase, a total of 8 blocks were used with 6 of them getting

damaged completely after the test while in the second phase, a total of 9 blocks were used: 2 from the first phase while 7 were extra that were left by Mohammadi (2014).

All the concrete blocks used in phase I were prepared following the guidelines provided in ASTM C192/ 192M – 06. These specimens were made from fresh concrete which was donated by a commercial concrete mixer. Fresh concrete was poured into 152 mm x 152 mm x 533 mm plastic forms to make concrete blocks. The forms were filled with concrete to the top followed by sufficient vibration to eliminate any air pockets and to ensure that it fills the form. Extra concrete was filled in 142 mm x 305 mm cylinders, to prepare specimens for both compressive and tensile tests. Both concrete cylinders and blocks were covered with a polythene film and kept in the lab for 28-day curing. Table 3.1-1 shows the results from both compressive and split tensile tests after 28-day curing.

Table 3.1-1: *Compressive and Tensile strengths for 28-day concrete*

	Compression Test		Split Tensile Test	
Specimen #	**Load (kN)**	**Stress (MPa)**	**Load (kN)**	**Stress (MPa)**
1	646.48	35.44	246.47	3.38
2	624.19	34.23	283.95	3.89
3	616.65	33.82	272.12	3.73
4	-	-	254.70	3.49
Average		**34.50**		**3.62**

The compressive strength was obtained directly from the Forney compression machine (Fig. 3.1-1); however, the split tensile strength was obtained using the following equation:

$$\sigma = \frac{2P}{\pi LD} \qquad (\mathbf{E3.1-1})$$

where, P is the measured load, while D and L are diameter and length of the specimen respectively.

On the other hand, seven of the specimens tested in phase II were prepared using concrete made in the lab with mixture proportions as shown in Table 3.1-2. Table 3.1-3 shows recorded compressive strength for the specimens by Mohammadi (2014).

Table 3.1-2: *Proportions of concrete mixture*

Water (kg)	128
Cement (kg)	279
Coarse Aggregate (kg)	887
Fine Aggregate (kg)	478
Air-entraining admixture (g)	164

Table 3.1-3: *Compressive strength for the 7 concrete blocks used in phase II*

Cylinders	Age (days)	Compressive Strength (MPa)	Average Strength (MPa)
M1-1		31.61	
M1-2	14	31.77	31.57
M2-1		31.27	
M1-3		32.41	
M2-2	28	32.23	32.93
M2-3		34.16	

Fig. 3.1-1: *Forney compression and tension test machine*

Strengthening Elements

Strengthening elements used in the current study include Tyfo UC® laminate strips, Tyfo S® and Tyfo TC® Epoxy adhesive. Tyfo UC laminate is a very high strength carbon composite material while Tyfo S® primer is a compound made of two components, type A and B, which were to be mixed in the ratio 100: 34.5 by weight. Application of this bonding element was done as per manufacturer's directions. Similarly, Tyfo TC ® is a two-component adhesive element: A and B, which were to be mixed by weight in the ratio 100:23.3 and applied to concrete substrate as per the manufacturer's directions. The table below shows critical properties of the strengthening elements.

Table 3.1-4: *Properties of Strengthening Elements*

Property	Tyfo® UC Laminate Strip	Tyfo® S	Tyfo® TC
Ultimate Tensile Strength (MPa)	2790	72.4	22.7
Tensile Modulus (GPa)	155	3.18	1.2
Layer Thickness (mm)	1.5	-	1.0
Elongation at break (%)	1.8	5.0	1.88

Concrete Surface Preparations

Water Grinding Process

The goal of this process was to remove the top weak layer off the concrete specimens in order to expose the coarse aggregate that would provide a strong bond between concrete and FRP. This was done using a water hand grinder shown in Fig. 3.1-2. By holding the grinder at an angle (< 30°), the grinder was pressed hard on concrete specimen until the top weak layer (1-2 mm) was removed. Specimens were then allowed 24 hours to dry.

Fig. 3.1-2: *A hand water-grinder and grinded specimens*

Groove Cutting Process

The next step involved marking groove lines on the specimens following diagrams shown in Fig. 3.1-3. Based on effective bond length calculations, it was observed that six grooves with a minimum of 50 mm spacing would be sufficient. Thus, six groove lines that were 50 mm apart were marked. However, the first groove line was marked 75 mm from the edge of the beam to accommodate the first 25 mm pre-crack condition. As shown in Fig. 3.1-4, the six black lines represent the groove lines while the red line represent the end of pre-crack condition.

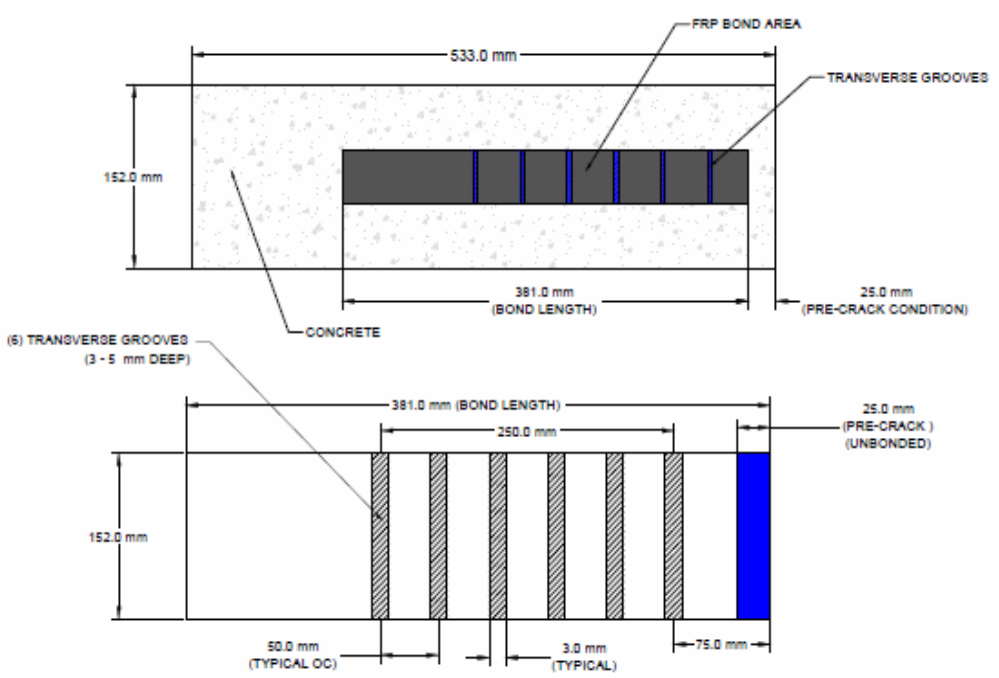

Fig. 3.1-3: *Groove cutting, bond area, and pre-crack condition dimensions*

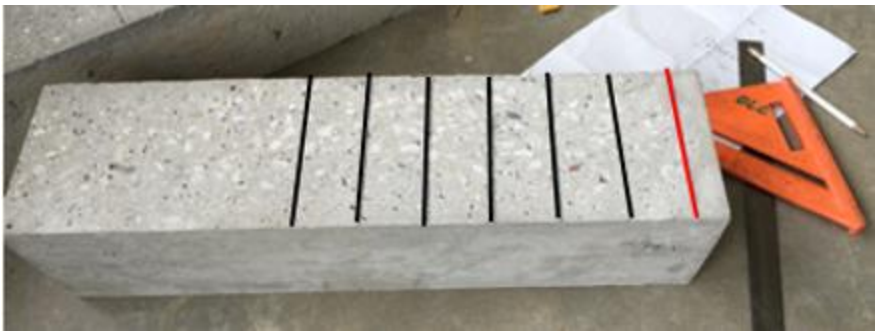

Fig. 3.1-4: *Groove and pre-crack condition lines marking*

Six specimens were grooved in each phase. Using a cutting machine, six groove-cuts were made on each specimen as shown in Fig. 3.1-5. Specimens in phase I were given 24 hours to dry up after cutting grooves. Specimens in the second phase were cleaned up using cold water together with a steel brush after cutting grooves, as shown in the Fig. 3.1-6. This process was to help eliminate any dirt or dust particles from the grooves and on the surface of the specimens. It also ensured that the specimens were well roughened to ensure a strong bond between FRP and concrete. After cutting and cleaning, the specimens were allowed 24 hours to dry.

Fig. 3.1-5: *Specimens with cut grooves*

Fig. 3.1-6: *Specimens cleaning using cold water and steel brush*

Air Pressure Cleaning, Waxing and Taping Process

Air pressure cleaning was to further clear any dry dust or tiny concrete particles which would otherwise compromise the bond strength. Six specimens were classified as either filled (F) or unfilled (U) by waxing them differently as seen in Fig. 3.1-7. The remaining were classified as control (C). For filled specimens, wax was applied on the outer sides – 50.5 mm from either side of the bond length, leaving the center region – 51 mm –where epoxy would be applied. For the unfilled specimens, wax was applied in all the grooves to prevent the epoxy from getting into them.

Lastly, taping was done on the outer sides of all the specimens leaving the area where the FRP would be bonded, as can be seen in Fig. 3.1-8. The goal of this step was to help minimize epoxy spills on the entire specimen during bonding process.

Fig. 3.1-7: *Waxed filled (F) and unfilled (U) specimens*

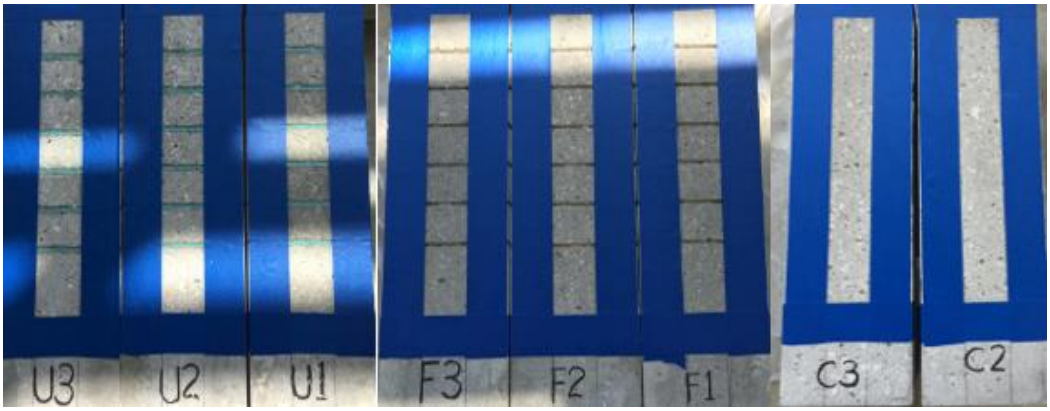

Fig. 3.1-8: *Taping specimens before application of epoxy*

Table 3.1-5 shows a summary of dimensions for the concrete specimens, FRP, and cut grooves

Table 3.1-5: *Concrete, FRP and Groove Dimensions*

		FRP Dimensions (mm)			FRP Dimensions (mm)			Groove Dimensions (mm)		
Phase	**Specimen**	**Length**	**Width**	**Height**	**Length**	**Width**	**Thickness**	**Length**	**Width**	**Depth**
I	C1; C2	533.0	152.0	152.0	711.2	51.0	1.5	-	-	-
	F1	533.0	152.0	152.0	711.2	51.0	1.5	152.0	3.0	3.1
	F2									4.0
	F3									3.2
	U1	533.0	152.0	152.0	711.2	51.0	1.5	152.0	3.0	3.2
	U2									3.2
	U3									3.2
II	C3; C4; C5	533.0	152.0	152.0	711.2	51.0	1.5	-	-	-
	F4	533.0	152.0	152.0	711.2	51.0	1.5	152.0	3.0	4.8
	F5									4.9
	F6									5.0
	U4	533.0	152.0	152.0	711.2	51.0	1.5	152.0	3.0	4.9
	U5									5.0
	U6									5.0

Preparation of Primer and Adhesive, and the Bonding Process

Prior to the bonding process, both the adhesive and the primer epoxies were prepared. Tyfo® S, primer, was the first to be prepared as per the manufacturer's directions. 100 parts of component A was added into 34.5 of component B (by weight) and thoroughly mixed for five minutes with a low speed mixer at 400-600 rpm until the two components were uniformly blended. This compound was then applied to all the eight specimens as shown in Fig. 3.1-9. The purpose of applying this compound first was to fill the micro-cracks in concrete in order to ensure a solid surface for bonding FRP and to also ensure quality bonding between FRP and concrete. Grooves on the filled specimens were also filled with primer. Once applied, the specimens were given at least 24 hours to cure after which the adhesive was applied.

Tyfo® TC Epoxy, Tack Coat adhesive was used as a coating compound. Like Tyfo® S, this compound was prepared following manufacturer's directions. This compound was mixed using weight ratio: 100.0 parts of component A to 23.3 parts of component B. The compound was then thoroughly mixed for five minutes at a speed of 400-600 rpm. This was then followed by applying the compound on all the specimens. A hand roller was used to apply the adhesive on the bond area of all the specimens as can be seen in Fig. 3.1-10.

An extra thin layer of the adhesive was applied to FRP after which the two materials were bonded together. FRP was carefully placed on the bonding area of concrete, lightly pressed until extra adhesive came off through the sides as seen in Fig. 3.1-11. This was to help ensure that any air pockets are removed and a uniform bond thickness between concrete and FRP is achieved.

Fig. 3.1-9: *Curing of specimens after application of Tyfo® S primer*

Fig. 3.1-10: *Application of Tyfo® TC Epoxy adhesive*

Fig. 3.1-11: *Bonding FRP to concrete*

Summary of Surface Preparation Method

Below are summarized steps of concrete surface preparation leading to bonding process.

- Water Grinding – This process is aimed at removing the top weak layer of concrete using a hand grinder attached with a rough circular rubber pad. The grinder is held at an angle to ensure efficient concrete removal.
- Groove Cutting – This is the process of cutting grooves in the concrete specimens using a cutting machine so as to obtain grooves in which additional epoxy can been added to enhance strength, in the case of F specimens.
- Air Pressure Cleaning, Waxing, and Taping – This involves running a high stream jet of air in the grooves to expel any concrete dust or tiny particles. Waxing is done to establish regions that need to be filled with epoxy from those that do not. Taping is the conducted to help minimize epoxy spillage on the specimens
- Primer and Adhesive Preparation and Application – Both the primer (Tyfo® S) and the adhesive (Tyfo® TC) are prepared as per the manufacturer's directions and applied on the concrete bond regions before attaching FRP.

Strain Gauge Attachment Process

Once the TC epoxy had cured for at least 72 hours, strain gauges were attached on the specimens. During this process, locations where strain gauges would be placed were marked off on the FRP with the help of Fig. 3.1-12. The first strain gauge was attached on the unbonded region of the FRP while last gauge was attached towards the end of the bond. Note that different specimens had different number of strain gauges.

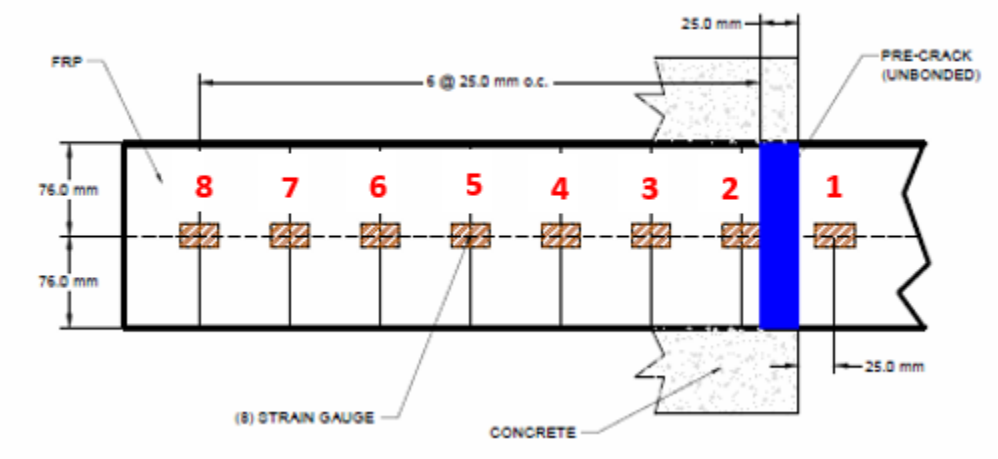

Fig. 3.1-12: *Proposed strain gauge locations*

3.2 SINGLE SHEAR PULL OUT TEST SET UP

Single shear pull-out test is one of the most common used method to determine the bond behavior between FRP and concrete. In the current study, single shear pull-out test is chosen to help determine the bond behavior for transversely grooved concrete specimens bonded with CFRP plate laminates because the method employs few materials and is relatively easy to set up.

Testing Equipment Set-up

To fully understand the bond behavior between FRP and concrete, a half of concrete beam (Fig. 3.2-1) was considered for the pull-out test. A pre-crack notch, which is half the depth of the beam, was created in the beam mid-span to mimic a flexural loading crack. The single shear pull-out test specimen had dimensions of 152 mm wide x 152 mm high x 533 mm long (Fig. 3.2-2).

The steel tube (HSS 203 x 254 x 9.8) in Fig. 3.2-3 has a small vertical plate (half the beam depth) welded on it that acts as a horizontal constraint. The beam is then firmly held on the steel tube by using the clamping system – uplift constraint system, which prevents the beam from lifting during the test.

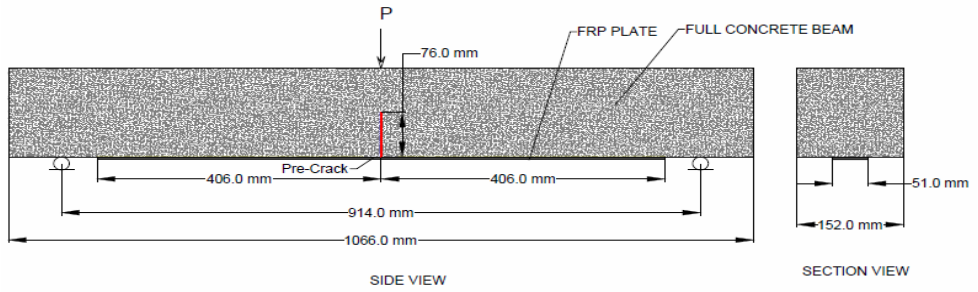

Fig. 3.2-1: *Beam dimensions together with pre-crack condition (Mohammadi, 2014)*

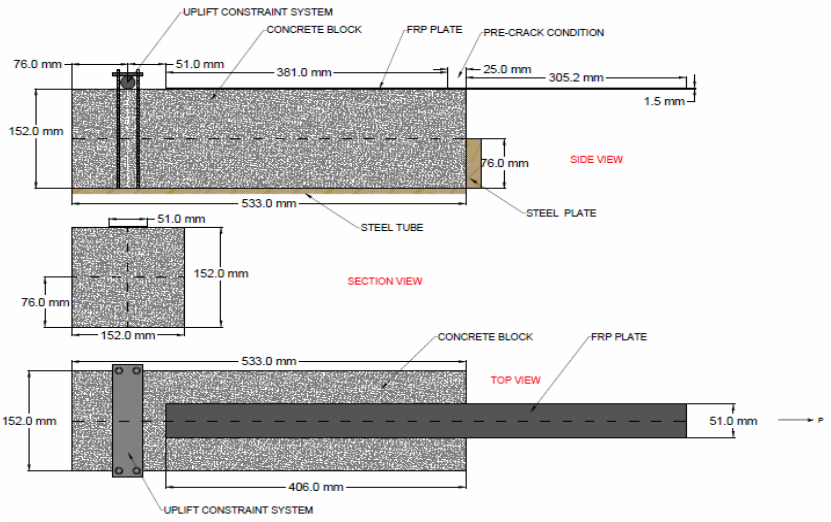

Fig. 3.2-2: *Concrete half-beam dimensions*

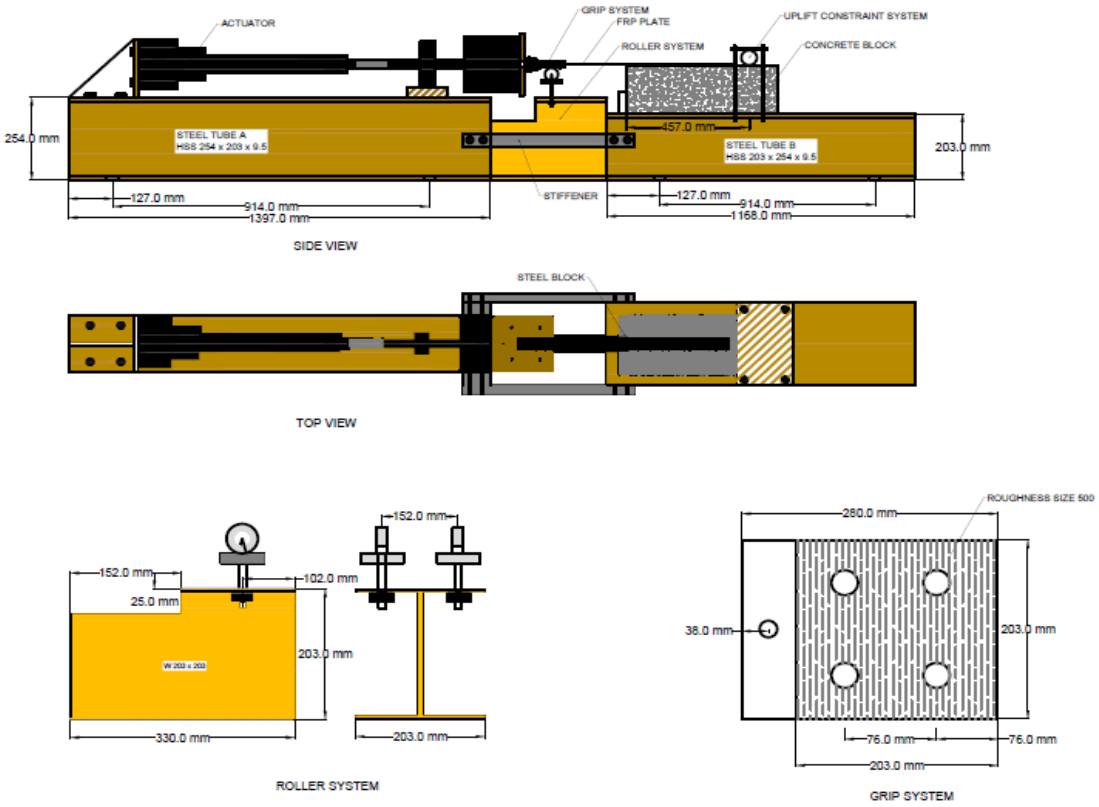

Fig. 3.2-3: *Single shear pull-out test equipment*

A hydraulic actuator (model **201.20T**) from Minnesota Testing Systems (MTS) Company is used to pull the FRP plate off the concrete substrate. The actuator is placed on the opposite side of the concrete specimen in order to pull the FRP from concrete until failure.

The two steel tubes on which the concrete specimen and actuator are sitting on are firmly bolted on the floor to refrain any movement during the pull-out test. To further restrict any horizontal movement between the two tubes, two steel stiffeners are bolted between them, allowing the whole setup to be firmly locked on the floor. Between the two steel tubes there is a roller system which is made of a W 203 x 203 (mm) beam that has two aluminum roller wheels bolted to it. The rollers help ensure that the specimen and the actuator are leveled up for uniform pulling since they are free to move up and

down. The rollers also ensure minimum friction between the grip system and the roller system during the pull-out test. The grip system is bolted on the actuator. This system is made up of two plates, PL 280 x 203 x 25 (mm). The two plates are roughened on their inner faces to increase friction and to allow a tight grip with the FRP during pulling. The two plates are bolted together, with FRP between them. During the test, this grip system rests on the two rollers on the roller system. Fig 3.2-4 shows the actual test set up.

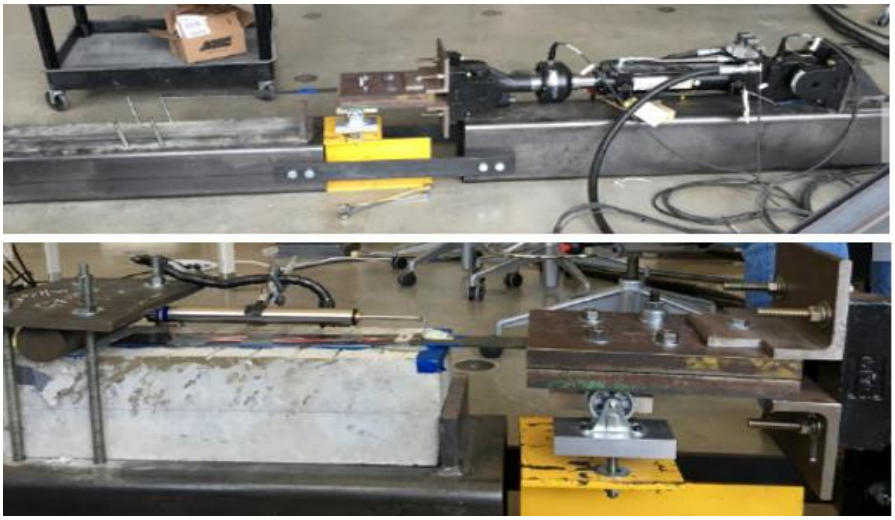

Fig. 3.2-4: *Single shear pull out test set up*

3.3 DATA ACQUISITION SYSTEM SETUP

Understanding the bond behavior for all control, epoxy-filled, and unfilled grooves specimens called for data acquisition system setup. Two data acquisition systems were put in place: Minnesota Testing Systems (MTS) and National Instruments (NI) systems. Since NI system recorded load and displacement like that recorded by the MTS, the data from the MTS was simply used for double checking purposes. And so, all the

critical data, load, displacement, strain gauge reading, and relative displacement, were acquired from the NI system.

National Instrument (NI) System Setup and Data Acquisition

The first step towards ensuring that some of the data is effectively collected from NI system involved gluing a small steel plate (65 mm x 50 mm) on every concrete specimen as shown in Fig. 3.3-1. The plate was strategically glued at 99 mm from the free edge and 55 mm from the top of the specimen to ensure that it does not prevent cracks that develop near the free edge during the pull-out test. The purpose of this steel plate was to hold the magnetic stand from which Linear Displacement Sensor (LDS) was mounted. Fig. 3.3-2 shows displacement sensor and strain gauges on the specimen during the test.

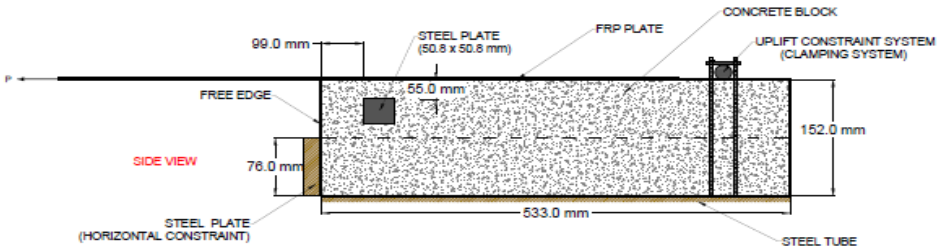

Fig. 3.3-1: *Steel plate location on the specimen setup*

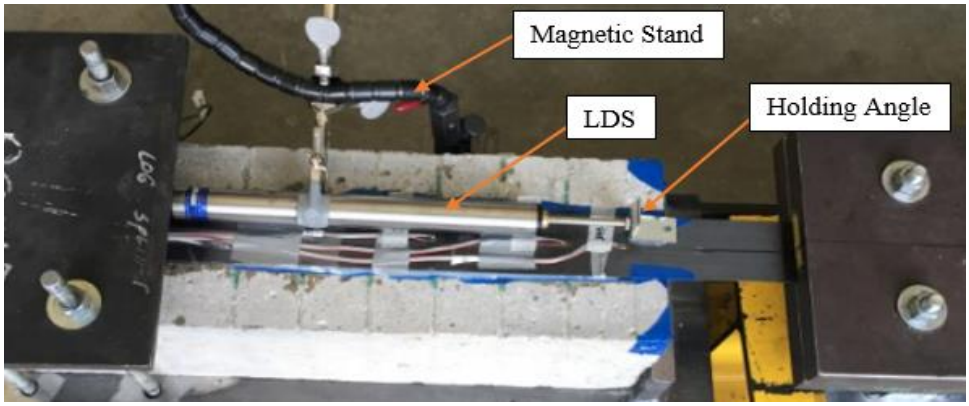

Fig. 3.3-2: *Linear Displacement Sensor mounted on the test specimen*

Liner Displacement Sensor Connection

Linear Displacement Sensor (LDS) was mounted on the test specimen as shown in Fig. 3.3-2. The purpose of this equipment was to measure relative displacement between concrete and FRP during the shear pull out test. Fig. 3.3-3 and Table 3.3-1 show the features of the sensor used in the test as provided by the manufacturer, Micro-Measurements®

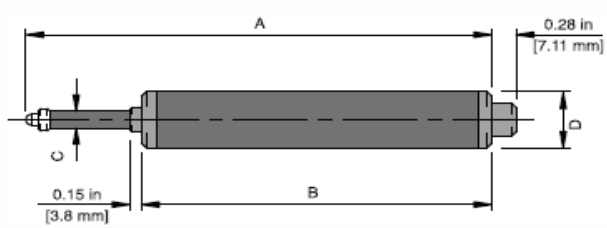

Fig. 3.3-3: *Linear Displacement Sensor, LDS*

Table 3.3-1: *Properties of LDS*

Model	HS 100
Displacement Range (mm)	102
Dimension A; B; C; D (mm)	380.2; 266.0; 6.0; 25.4
Weight (g)	500
Spring force (g)	350
Excitation (ac or dc)	2 to 10 V
Frequency Response	5-mm displacement: 100 Hz; 100-mm displacement: 10 Hz
Rate (F.S) Output	5.2 mV/V
Resolution	Infinite
Bridge Resistance	350 ohms Bridge, 100k ohms Zero Balance
Temperature Range (°C)	-10 to +60
Electrical connections	**Input:** Red+ Black-; **Output:** Green+ White-

The equipment has infinite resolution, true output linearity over the entire measurement range, low operating forces, and an excellent stability and temperature

compensation as pointed out by the manufacturer. Once it was hooked to the specimen, the LDS was connected and configured in the NI system software as shown in Fig 3.3-4.

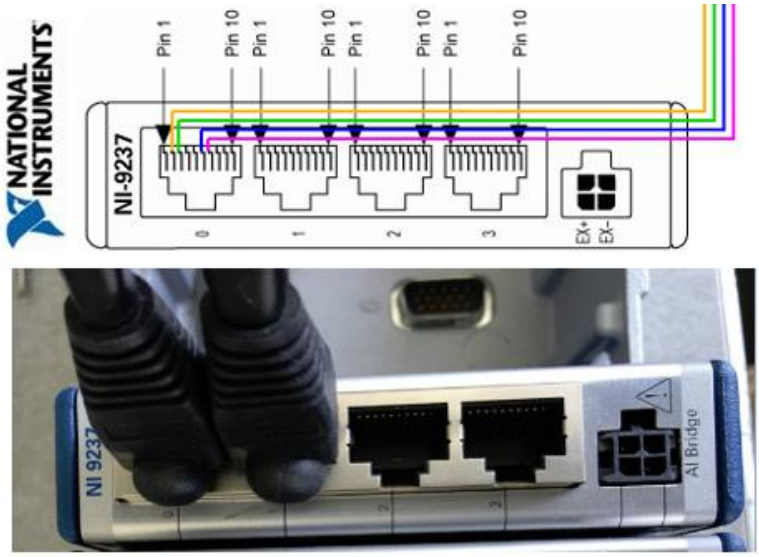

Fig. 3.3-4: *Connection of LDS to NI data collection system*

In the NI software configuration window, some of the properties of the LDS (Table 3.3-1) were entered as shown in the Fig 3.3-5 ("**MM POT PCC**")

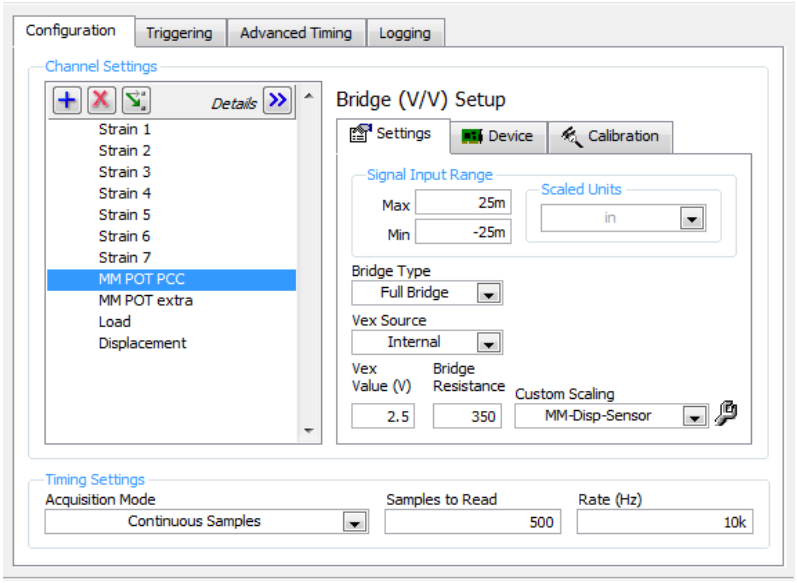

Fig. 3.3-5: *Configuration of LDS into NI system*

Strain Gauge Connection

Strain gauges were glued at designated locations along the FRP length to help determine the strain variation along the FRP-concrete interface. These were general purpose gauges – Linear Pattern (**CEA-06-062UW-350**) from Micro-Measurements® (Fig. 3.3-6). Note that these gauges were used in phase I. For phase II, gauges bought from China with similar properties as those from Micro-Measurements® were used. Strain gauges used had properties shown in Table 3.3-2.

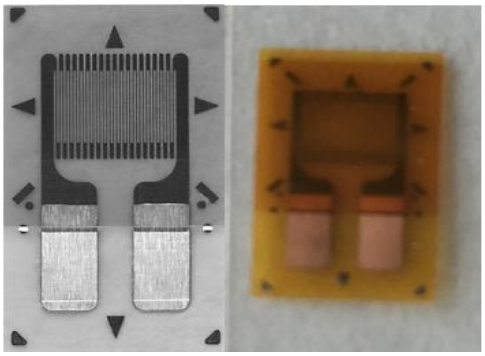

Fig. 3.3-6: *General Purpose Strain gauge*

Table 3.3-2: *Strain gauge properties*

Gauge Length (mm)	1.57
Overall Length (mm)	5.59
Grid Width (mm)	3.05
Overall Width (mm)	3.05
Matrix Length (mm)	7.90
Matrix Width (mm)	4.80
Grid Resistance (ohms)	350.0±0.3 %
Gauge factor @ 24°C	2.210±0.5 %
Transverse Sensitivity	(+0.7±0.2) %
Strain Range	±3 %
Temperature Range (°C)	-75 to +175

Wires were then soldered on to the gauges and hooked into the NI system box as shown in Fig. 3.3-7.

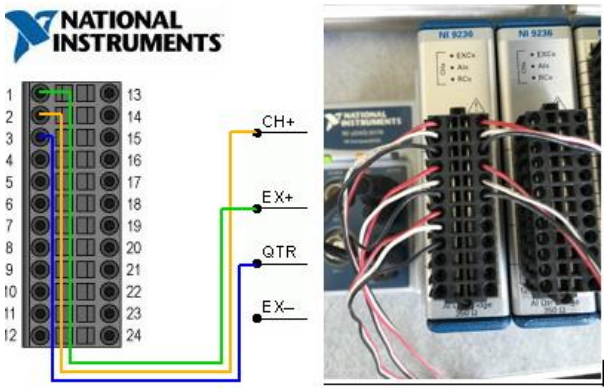

Fig. 3.3-7: *Strain Gauge Connection*

After completion of the connection shown in Fig 3.3-7, configuration of all strain gauges was performed in the NI system software as shown in Fig. 3.3-8 using some of the properties shown in the Table 3.3-2.

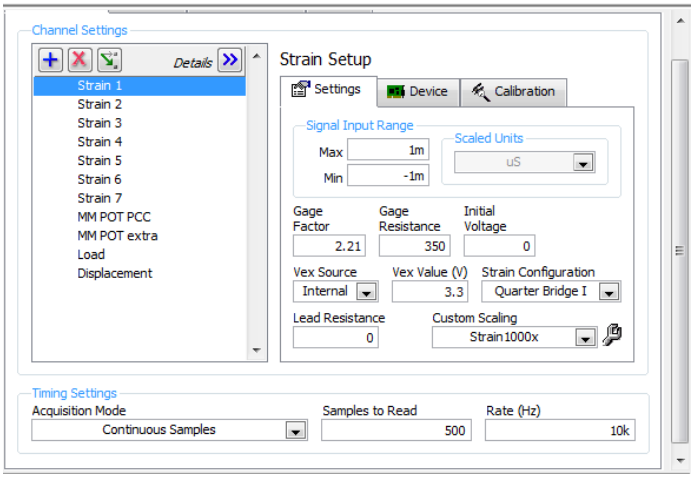

Fig. 3.3-8: *Strain Gauge Configuration in NI System*

MTS System Configuration into NI System

The MTS system, which was responsible for controlling the actuator that pulls the test specimen, was also configured into the NI system. Fig. 3.3-9 shows configuration of the actuator into the NI system. The load was configured using holes **1** and **17** while the displacement was configured using holes **2** and **17.**

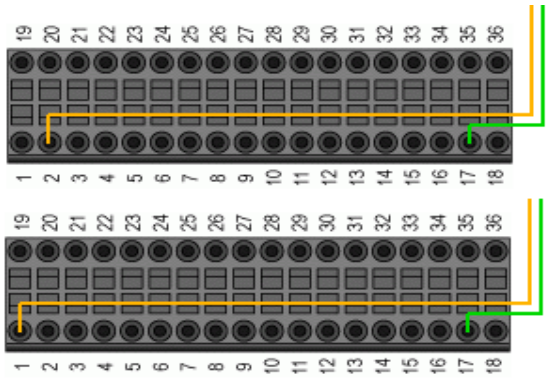

(a) *Load and Displacement Configuration*

(b) *Load and Displacement actual connection*

Fig. 3.3-9: *Configuration of MTS load and displacement to NI*

In the NI software, settings shown in Fig. 3.3-10 were made for both load and displacement for the actuator.

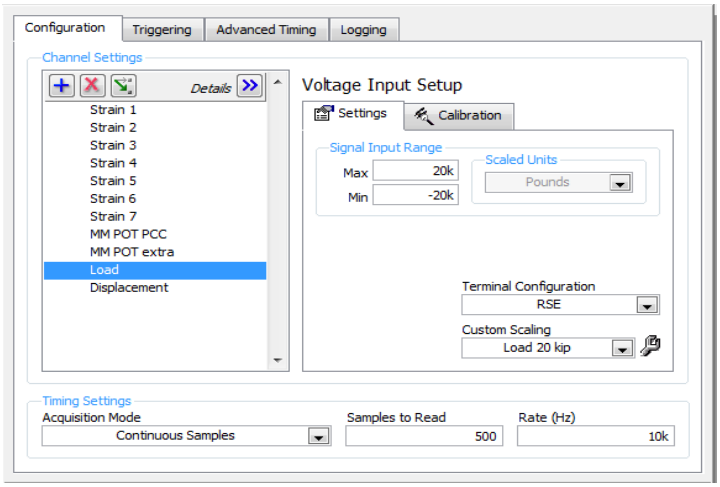

Fig. 3.3-10: (a) *Load configuration in the NI system*

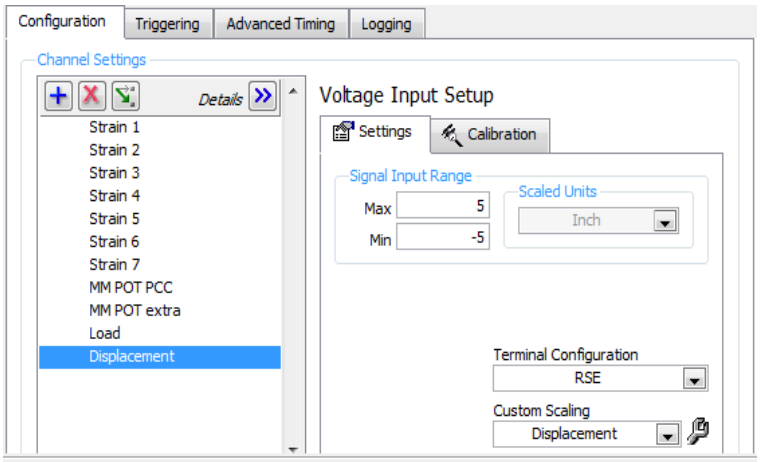

Fig. 3.3-10: (b) *Displacement configuration in the NI system*

Once all the configurations and settings were done, all specimens were tested, data collected and analyzed as shall be discussed in the following sections.

3.4 OBSERVATION AND DISCUSSION OF EXPERIMENTAL WORK

By the end of the experiment, a total of 17 specimens had been tested, results collected and analyzed as shall be discussed in the paragraphs to follow. Five (5) specimens were tested as control (C), 6 as unfilled (U) and 6 as filled (F). As already mentioned in the previous sections, all the tests were conducted under ***single shear pull-out test***.

Control Specimens (C)

The purpose of these specimens was to act as reference to both unfilled and filled specimens. Five specimens were tested as control: C1-C5. Data collected after each test

was analyzed and plotted as load-strain, strain-displacement and load-displacement. However, out of the five specimens, only one was successful: C5.

Specimens C1-C4

Specimens C1, C2, and C3 failed by FRP splitting even after some being tested for a second time. This failure was such that, during the test, a small section of the of the FRP (less than 6 mm in width) split off the entire FRP. Such failure was believed to have been caused by uneven torque applied on the four bolts holding the steel plates that hold the FRP in position during the test. Since a hand wrench was used in tightening these bolts, equal torque could not be guaranteed.

Such unevenness caused the FRP to be firmly held on one side and loosely held on the other. The side that was firmly held was thus the one being split off from the rest of the FRP. Following this development, a calibrated wrench together with an impact wrench were then employed. On the other hand, specimen C4 failed due to accidental damage before testing. Fig. 3.4-1 shows typical failure for specimens C1-C3.

Fig. 3.4-1: *Typical Split Failure for specimens C1-C3*

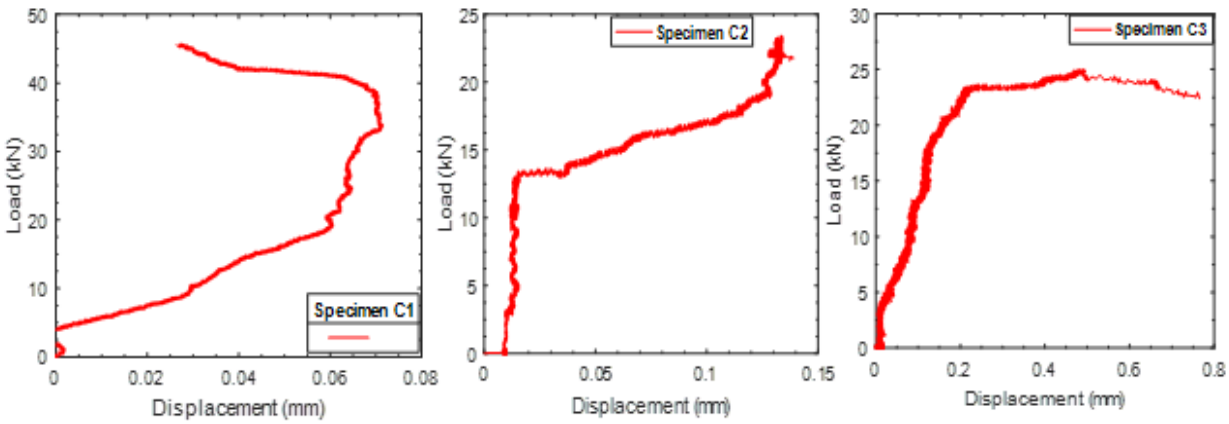

Fig. 3.4-2: *Load-displacement plots for specimens C1, C2, and C3*

Data from specimens C1, C2, and C3 were discounted in the analysis due to their irregularity and the fact that it was obtained after the specimens were tested twice. The load-displacement curves for C1, C2, and C3 are shown in Fig. 3.4-2.

Specimen C5

Specimen C5's data was used for comparison with the other successful specimens in both unfilled and filled categories. Fig. 3.4-3 shows plots and failure mode obtained from specimen C5.

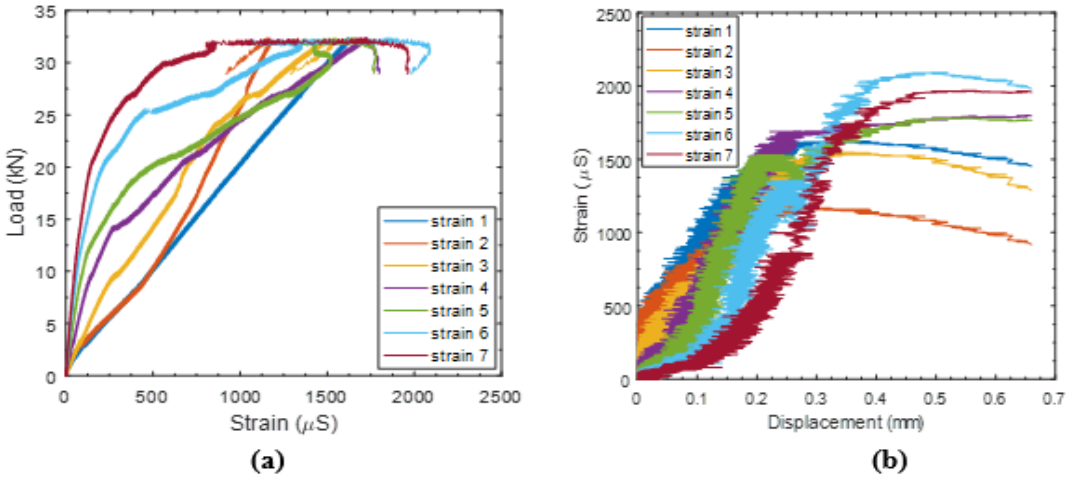

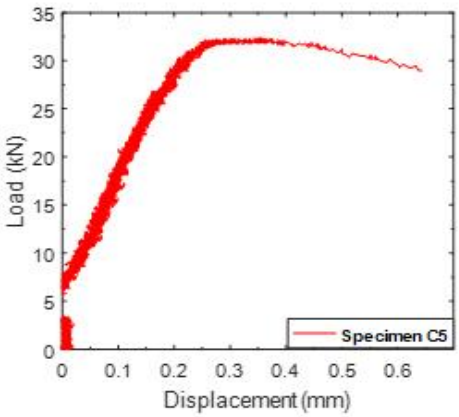

(c)

(d)

Fig. 3.4-3: *Specimen C5: (a) Load-Strain; (b) Strain-Displacement; (c) Load-Displacement* ***(c)****; and (d) Failure Mode*

From Fig. 3.4-3 (a), strain decreases from gauge 1 – 7 because of increasing debonding. Strain 1 has the largest strain with linear relation with the load because it is located on the unbonded region of the FRP. Fig. 3.4-3 (b) shows strain-displacement plot. All the curves on the plot indicate an increasing strain associated with increasing displacement. As debonding progresses, FRP becomes more susceptible to pulling hence increasing displacement between concrete and FRP.

Load-displacement plot is shown in Fig. 3.4-3 (c). It is observed that FRP reaches maximum load and start debonding, which occurs at 32 kN followed by failure at 29 kN. Thus, it can be said that increasing the load causes micro-cracking in concrete that propagate parallel to the FRP-concrete interface that results in debonding.

Finally, failure mode for specimen C5 is shown in Fig. 3.4-3 (d), which is observed to be debonding. Not only does FRP debonding happens but also concrete cracking, which is caused by the 45 degree cracks that are initiated near the pre-crack condition area. This phenomenon was also observed by Mohammadi (2014).

Unfilled Specimens (U)

This was the second group of specimens to be tested. Specimens in this group had grooves. However, these grooves were left open when the FRP was bonded to concrete hence the name *unfilled*. Six specimens were tested: U1-U6, out of which only two were unsuccessful (U1 and U2) while the rest successful (U3-U6).

Specimens U1-U2

While specimen U1 was successfully tested, however, the data collected was considered null due to irregularity due to the setup error in the NI system. Fig. 3.4-4 shows plots from specimen U1.

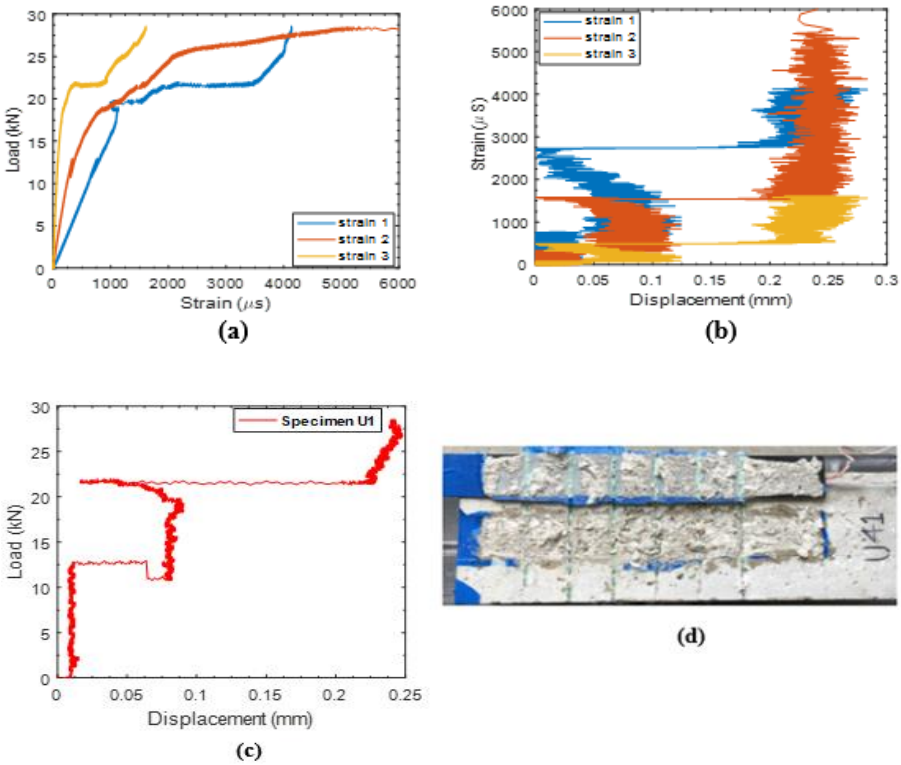

Fig. 3.4-4: *Specimen U1: (a) Load-Strain; (b) Strain-Displacement; (c) Load Displacement; and (d) Failure Mode*

Specimen U2 was tested, however, there was a glitch in the NI system resulting in no data collection. Thus, this specimen was ignored.

Specimen U3

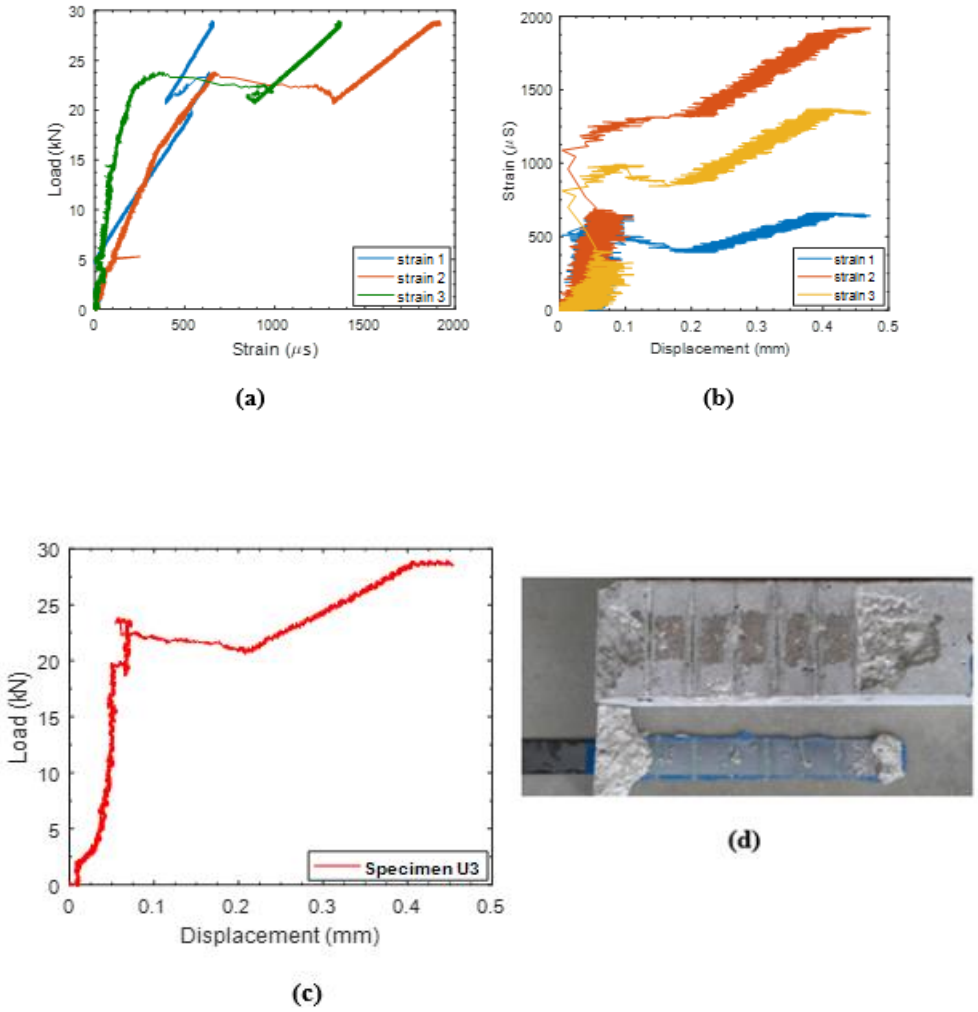

Fig. 3.4-5: *Specimen U3: (a) Load-Strain;(b) Strain-Displacement; (c) Load-Displacement; and (d) Failure Model*

As one of the successful specimen, U3's ultimate load is 29 kN. Between 20 kN and 23 kN there is a load drop as indicated by Fig. 3.4-5 (a). Such behavior is linked to

the possibility of FRP slipping out of the two plates holding it together due to either low friction in the two plates or the possibility of debonding.

Fig. 3.4-5 (d) shows specimen failure mode, which appear to be both concrete rupture and debonding. Angular rupture at the front of the specimen suggests angular cracks that propagated from the pre-crack condition during the test. Concrete rupture is also witnessed at the back of the specimen. After failure, it is observed that some of the concrete chunks are left on FRP. However, peeling of the FRP from the interface between FRP and concrete appear to have dominated in the middle section of the bond length. This may suggest poor surface preparation of concrete specimen. It may also be due to poor epoxy application

Specimen U4

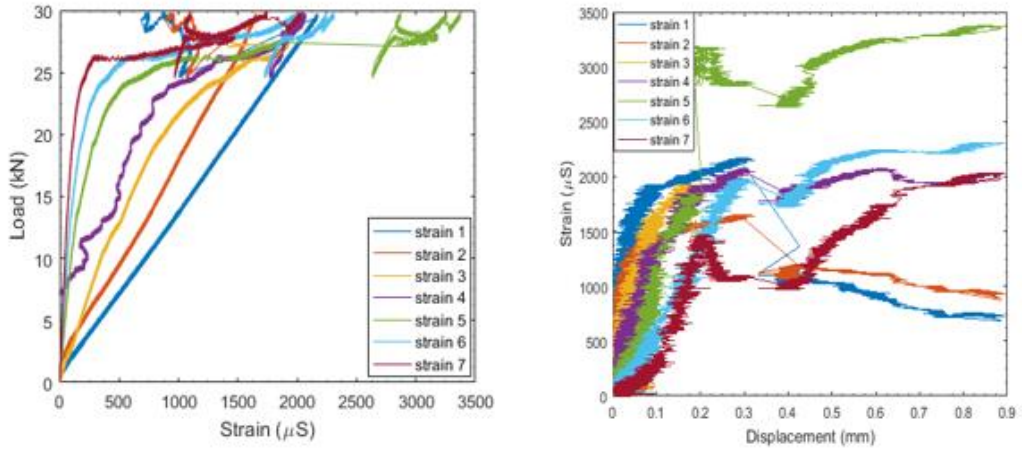

(a) **(b)**

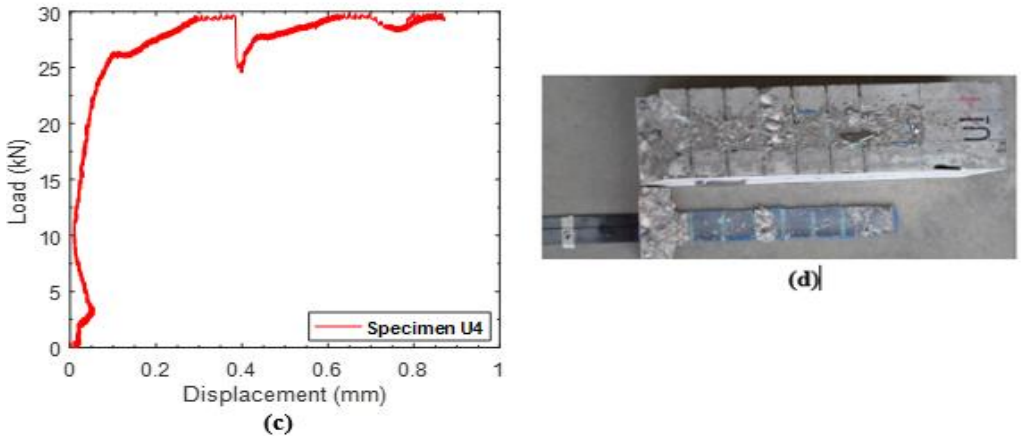

Fig. 3.4-6: *Specimen U4: (a) Load-Strain; (b) Strain-Displacement; (c) Load-Displacement; and (d) Failure Mode*

Specimen U4 recorded an ultimate [failure] load of 30 kN with FRP beginning to debond at 27 kN. Prior to debonding, load-strain relationship appears linear, however, past this point, the relation becomes nonlinear. Note that gauge 1 indicates a linear behavior throughout until failure because it is connected on the unbonded region of the FRP. Ultimate displacement is observed to be 0.89 mm.

Fig. 3.4-6 (c) shows load-displacement. Below 0.5 mm, the load curve looks s-shaped. Such behavior is attributed to slippage of FRP from the steel plates holding it in place or re-aligning of concrete on the steel tube as this occurrence happens in the early stages of loading.

Load drop is also observable, indicating debonding in areas presumed to have been poorly prepared during surface preparation process. Since the specimen lacks epoxy in the grooves, it is believed that such a drop in the load is because of peeling of FRP at regions that were poorly prepared. [Fig. 3.4-6 (c)].

Mixed mode failure is shown Fig. 3.4-6 (d). There is concrete rupture near the loading edge due to angular cracks that develop near this region, propagating down

towards the constrained face. Debonding in concrete, on the other hand, is witnessed at the middle and the end of the bonded length – which indicates strong quality bond between FRP and concrete. Failure in the mid-section of the bond seems to leave concrete undamaged. Such failure is attributed to either minimal surface preparation or poor epoxy application.

Specimen U5

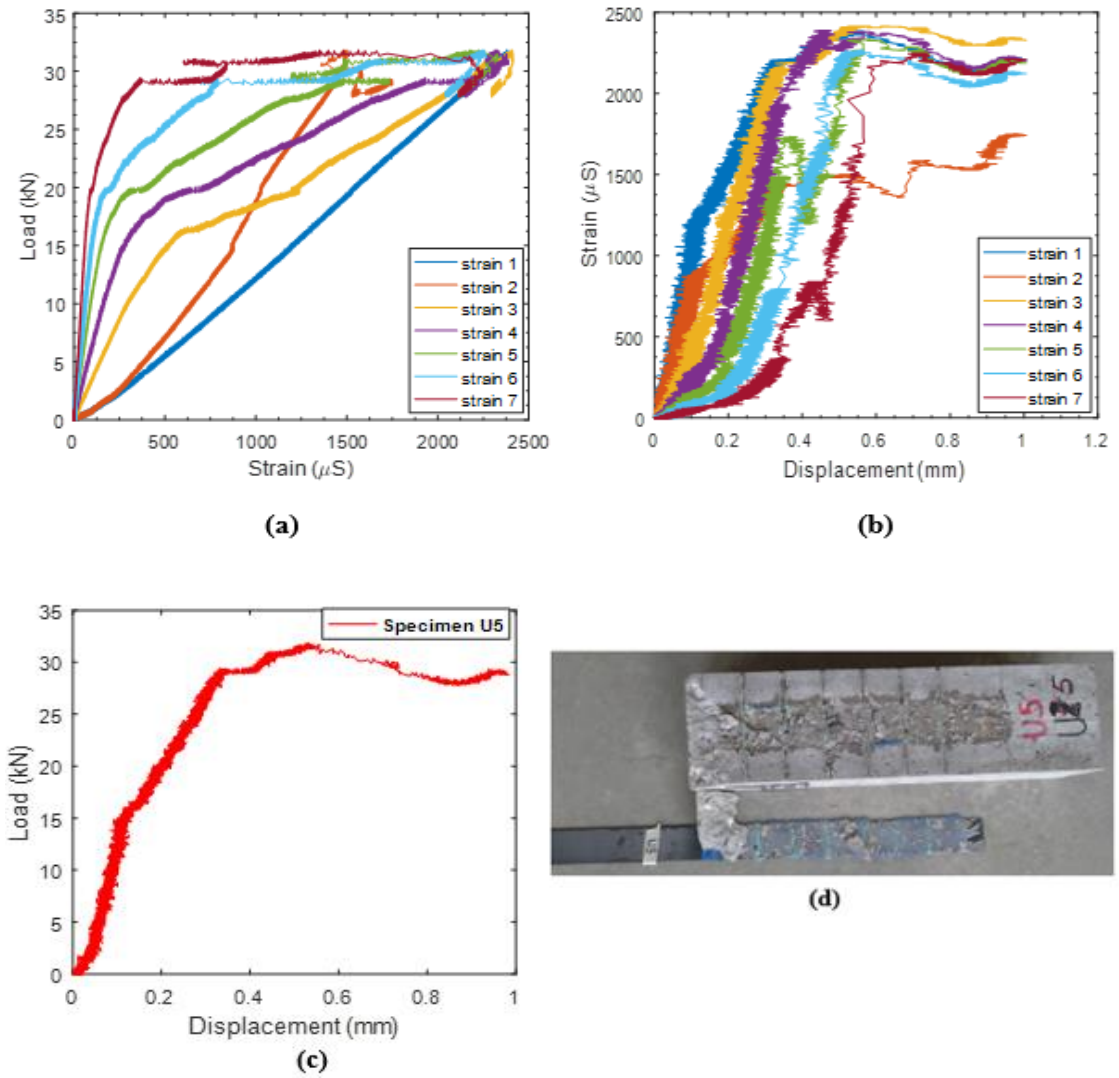

Fig. 3.4-7: *Specimen U5*: (a) *Load-Strain; (b) Strain-Displacement; (c) Load-Displacement; and (d) Failure Mode*

Like specimen U4, specimen U5 had seven strain gauges attached to it: six on the bonded length and one on the unbonded length, near the pre-crack condition.

From load-strain plot, Fig. 3.4-7 (a), ultimate load is 29 kN. Debonding seems to begin at 20 kN, as indicated by change in slope in strain gauges 2-7. This is the point where micro-cracks have already propagated into the FRP/concrete bond. It is also observed that the ultimate displacement is 0.98 mm. Maximum load is recorded at 32 kN. However, prior and after maximum load, there are few drops in the load, which indicate debonding.

Failure mode is depicted by Fig. 3.4-7 (d). Failure seems to be mixed mode: concrete rupture and debonding. Near the pre-crack condition, larger cracks that are caused by micro-cracks within concrete are propagated further down forming 45 degree angles. These cracks lead to rupture failure. However, the rest of the bond length witnesses debonding.

Specimen U6

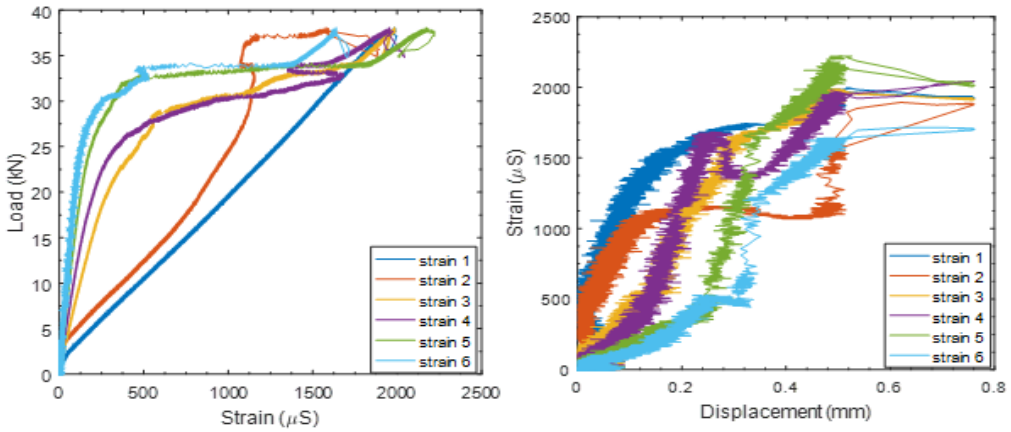

(a) **(b)**

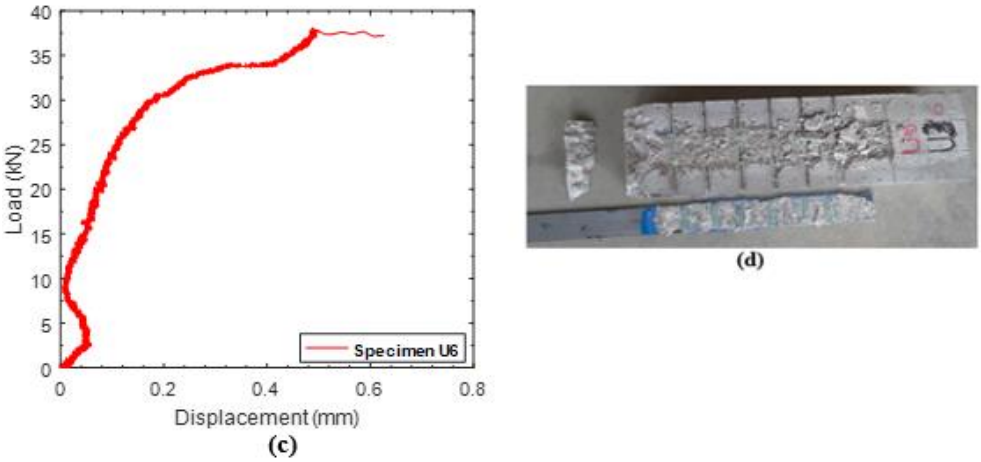

Fig. 3.4-8: *Specimen U6: Load-Strain; (b) Strain-Displacement; (c) Load-Displacement; and (d) Failure Mode*

From Fig. 3.4-8 (a), maximum load is observed at 38 kN. Debonding seems to start at 30 kN because of the changing slope. This is the point where micro-cracks are propagated into the bond interface leading to debonding of FRP off concrete substrate. Also, it is seen from Fig. 3.4-8 (a) that gauge 1 is linear all through, which is explained by the fact that the gauge is attached on the non-bonded region of the FRP.

Ultimate displacement is 0.7 mm while ultimate load is 37 kN, from Fig. 3.4-8 (b) and (c). The s-shaped behavior observed on specimen U4 is also observed on this specimen. Such behavior is suspected to have been caused by concrete realigning with the actuator or even the possibility of LDS erroneous movement on the angle that it is attached to.

Fig. 3.4-8 (d) shows failure mode. It is observed that debonding failure dominates. However, in front of the specimen, failure is due to rupture of concrete caused by 45 degree angular cracks that propagate from the pre-crack region towards the bottom of the concrete. Debonding failure indicates a perfect contact between concrete and FRP that results from quality surface preparation of the specimen.

Filled Specimens (F)

Specimens in this category had same physical features as those in unfilled category except that in this category grooves were filled with epoxy adhesive. Six specimens were tested, with only one being considered null: specimen F2.

Specimen F1

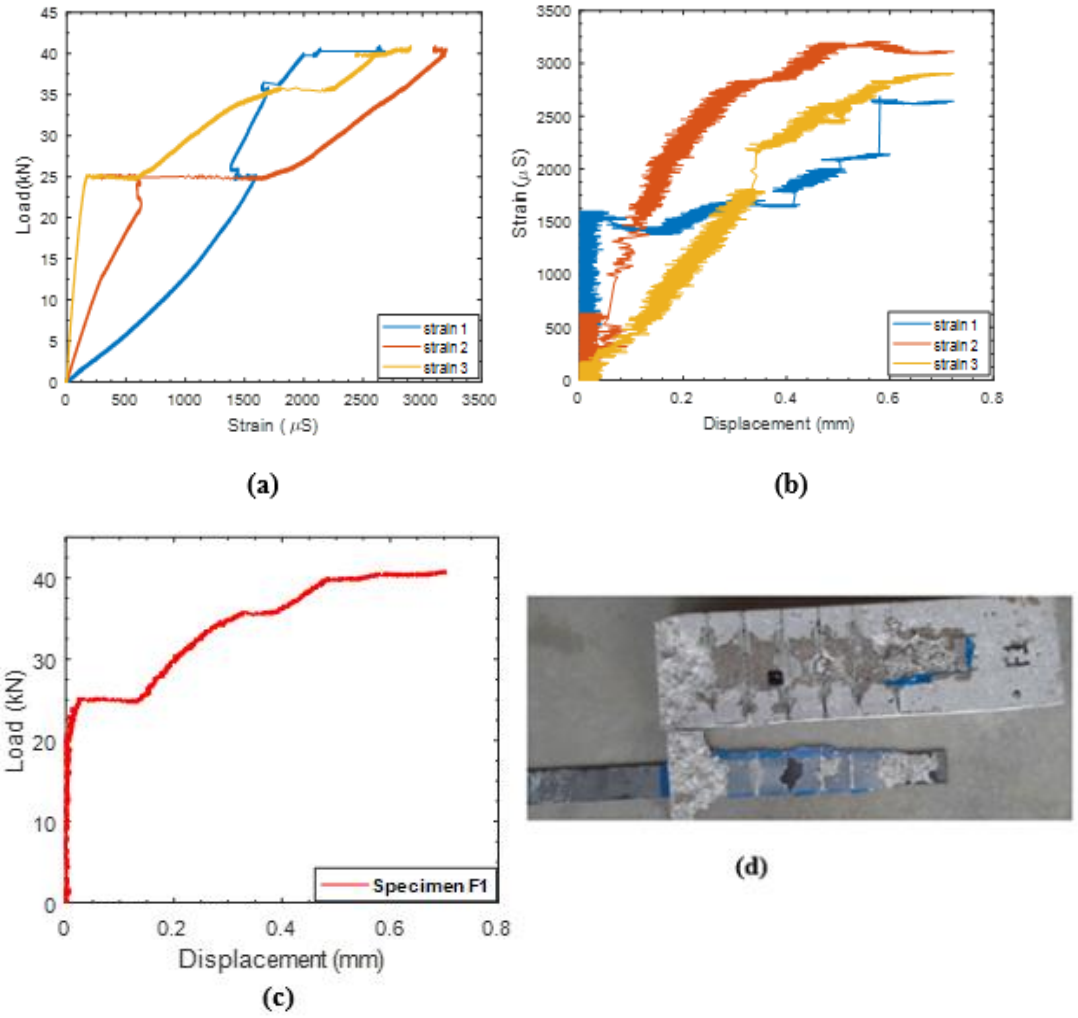

Fig. 3.4-9: *Specimen F1: (a) Load-Strain; (b) Strain-Displacement; (c) Load-Displacement; and (d) Failure Mode*

Specimen F1 had three strain gauges attached to it as shown in Fig. 3.4-9 (a). Ultimate load is observed to be 41 kN with displacement of 0.72 mm. Below 25 kN, the load strain correlation appears linear, however, above this load there is variation between strain and load. This is the point where debonding begins to happen because of increased stress in the bond interface.

It is from this Fig. 3.4-9 (a) that the importance of having epoxy in the grooves is observed: above 25 kN, the load appears to be increasing stepwise. Every time a groove is broken, the curve seems to change the slope, which is attested to the fact that the grooves offer an additional bond that requires extra load to break.

Fig. 3.4-9 (d) shows failure mode: debonding and rupture failures. The angular failure in front of the specimen suggests creation of 45 degree cracks created by progressive micro-cracks. Debonding failure is witnessed along the bond length where in some areas small chunks of concrete are left on FRP after failure while in other areas concrete stays intact. Limited surface preparation may be the cause of such failure i.e. concrete surface may not have been roughened up enough to create a strong bond between concrete and FRP.

Specimen F2

Data from this specimen was not used in comparison with the rest of the specimens due to inconsistency. Fig. 3.4-10 shows load-displacement and failure mode for specimen F2.

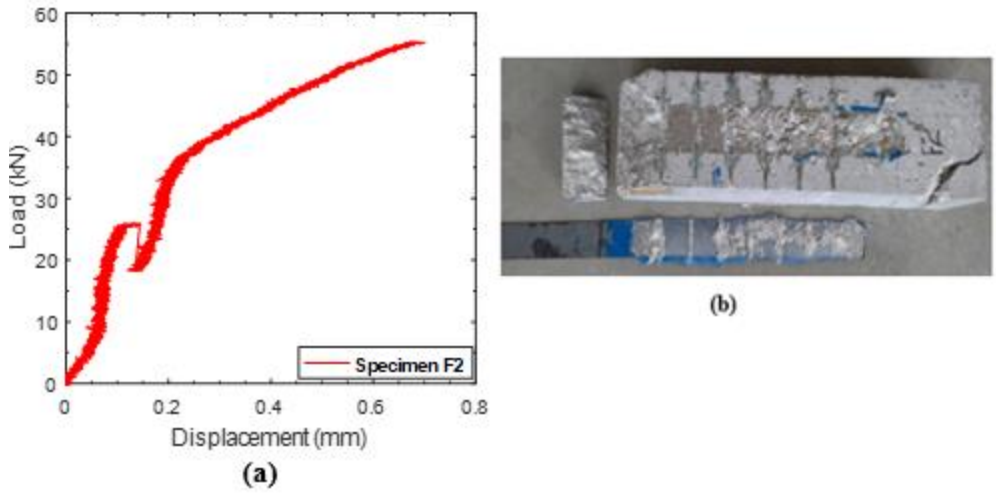

Fig. 3.4-10: *Specimen F2: (a) Load-Displacement; and (b) Failure Mode*

Specimen F2 was tested twice, however, data collected was rendered null. Ultimate load recorded by the specimen was 58 kN, as seen from the load-strain plot. This is the load at which the FRP was pulled off the concrete substrate.

While the data collected was null, however, failure mode observed include both debonding and concrete cracking. Due increased loading, micro-cracks continually develop in the concrete substrate. As these cracks grow bigger, they form 45-degree angle, originating from the pre-crack condition which results in rupture failure which is observed at the beginning of the concrete specimen.

On the other hand, debonding is witnessed along the bond length, where severe damage is witnessed from the third groove. Small concrete chunks are seen left on the FRP surface after failure. This failure is also seen inside some of the grooves, indicating the intended performance of the epoxy filled grooves i.e. to offer additional surface area that the bond must overcome during pulling.

Specimen F3

Specimen F3, like specimens F1 and F2 had three strain gauges attached to it. Plots and failure mode for specimen F3 are presented in Fig. 3.4-11.

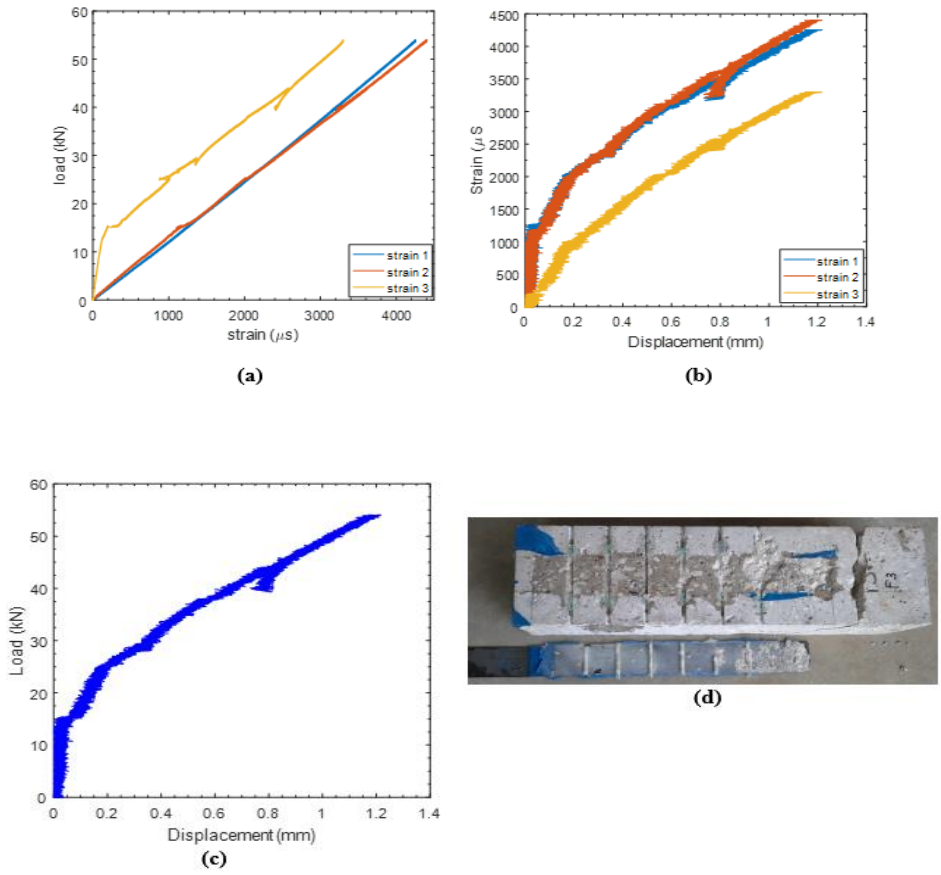

Fig. 3.4-11: *Specimen F3: (a) Load-Strain; (b) Strain-Displacement; (c) Load-Displacement; and (d) Failure Mode*

Ultimate load obtained by specimen F3 is 54 kN. Both gauge1 and 2 appear to display a linear relationship while gauge 3 displays similar behavior but with breaks which appear to occur regularly. Such breaks are believed to be caused by debonding in the grooves.

Fig. 3.4-11 (b) and (c) show two major drops in load: at 30 kN and at 43 kN. These drops occur at the fifth and the sixth groove as can be seen in Fig. 3.4-11 (d). There is a load drop for every filled groove that must be overcome during the debonding process. After failure, ultimate displacement is observed to be 1.22 mm. From Fig. 3.4-11 (c), debonding seems to start at 15 kN. Beyond this load, micro-cracking start to develop in concrete from bearing on the steel plate located in front of the specimen. These cracks are further propagated to the FRP-concrete interface causing the FRP to start debonding off the concrete substrate.

Failure mode is shown in Fig. 3.4-11 (d). Severe debonding is witnessed towards the end of the bond length where small concrete chunks are left on the FRP after failure. Minimal debonding is seen towards the beginning of the bond length, limited surface preparation prior to bonding. Like specimen F2, this specimen also broke towards the back due suspected tight clamping of the specimen on the steel tube during the test.

Specimen F4

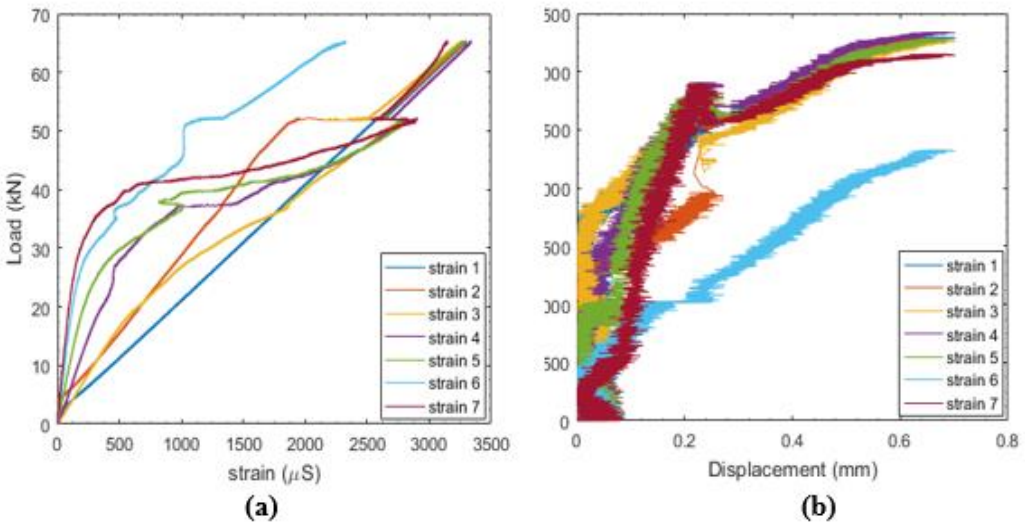

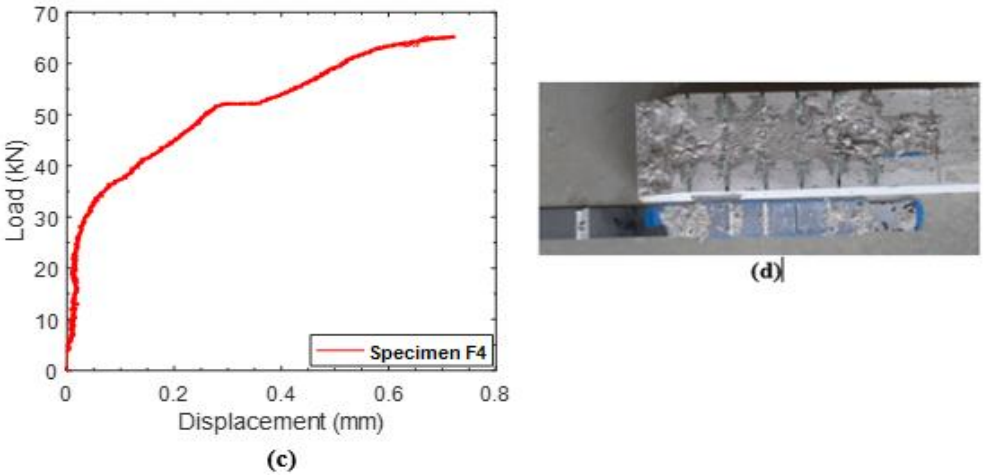

Fig. 3.4-12: *Specimen F4: (a) Load-Strain; (b) Strain-Displacement; (c) Load-Displacement; and (d) Failure Mode*

From the load-strain plot [Fig. 3.4-12 (a)], ultimate load is 65 kN. A linear correlation between load and strain is witnessed up to 30 kN. Past this load, the load-strain curves become nonlinear except strain gauge 1, which is located on the unbonded region of the FRP. This is the point where the debonding is assumed to be initiated.

Fig. 3.4-12 (b) shows strain-displacement relationship which indicates an ultimate displacement of 0.70 mm. On the same figure, there are two major load drops (at 52 kN and 65 kN), which indicate debonding in the groove areas as can also be seen from failure mode in Fig. 3.4-12 (d). Since all the grooves in the specimen are filled with epoxy, there is an added bond contact area and anchorage that must be overcome during pulling for failure to occur. Once a groove is debonded, there is a load drop.

Specimen F4's failure mode is mixed: concrete fracture and debonding. In front of the concrete substrate, there is a 45-degree fracture failure which can be attributed to the cracks that are initiated near the pre-crack condition area. These cracks grow bigger

towards surface of concrete near the bearing point. Severe debonding is witnessed the entire bond length, in which small chunks of concrete are left on the FRP after failure

Specimen F5

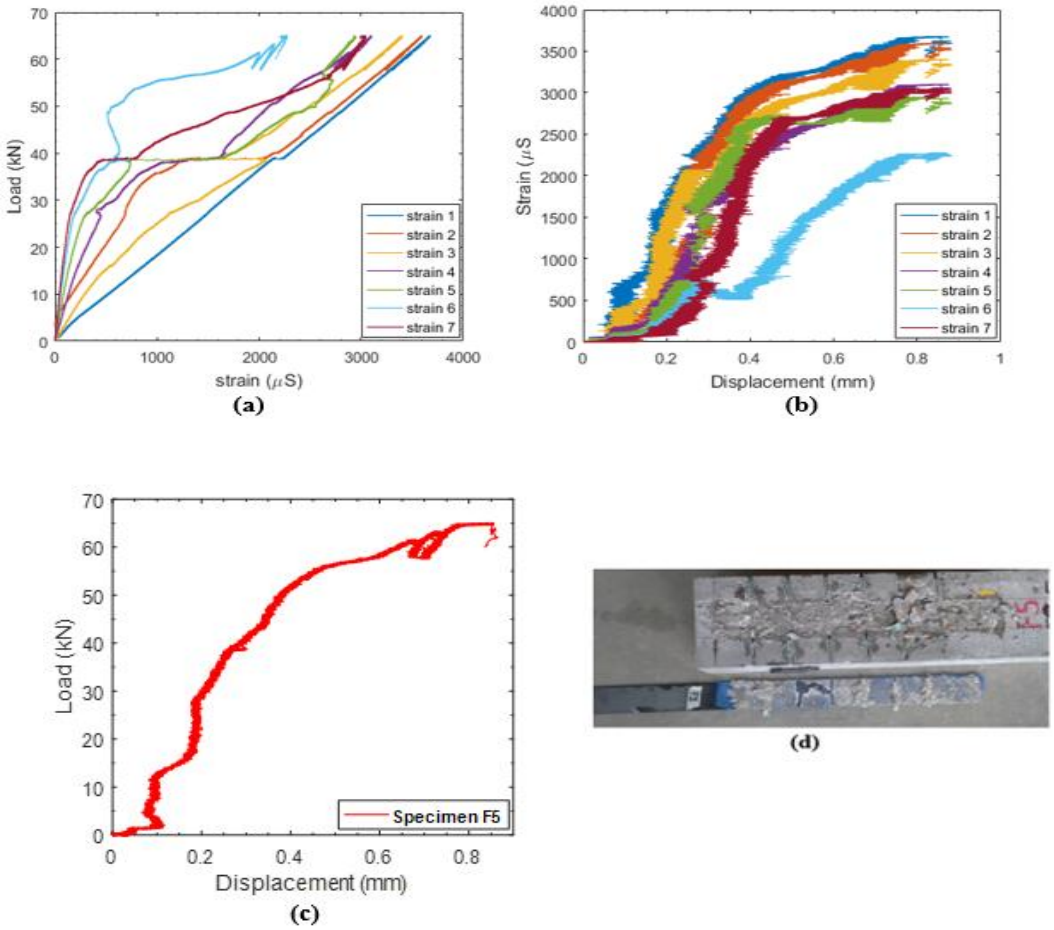

Fig. 3.4-13: *Specimen F5: (a) Load-Strain; (b) Strain-Displacement; (c) Load-Displacement; and (d) Failure Model*

For specimen F5, ultimate load obtained was 60 kN. Increasing load led to an increase in micro-cracks development. These cracks then propagated to the bond interface initiating debonding.

Ultimate displacement is observed to be 0.85 mm. As can be seen from Fig. 3.4-13 (c) there are two major load drops indicating debonding particularly in the bond grooves. The last two grooves on the specimen are assumed to be main cause of the drop. When debonding occurs in the grooves, there is a drop in the load as these grooves carry extra bond that need to be broken before the entire FRP fails. This is evidenced by the heavy damage on specimen's last two grooves Fig. 3.4-13 (d). S-shaped behavior is also seen in this specimen in the early stages of loading.

Failure mode is shown by Fig. 3.4-13 (d). Like other tested specimens in this category, failure mode is mixed. Debonding is witnessed the entire bond length with some areas debonded severely than others. The last two grooves seem to offer the strongest additional failure strength based on severe they are damaged. Concrete chunks are left on the FRP after failure.

Specimen F6

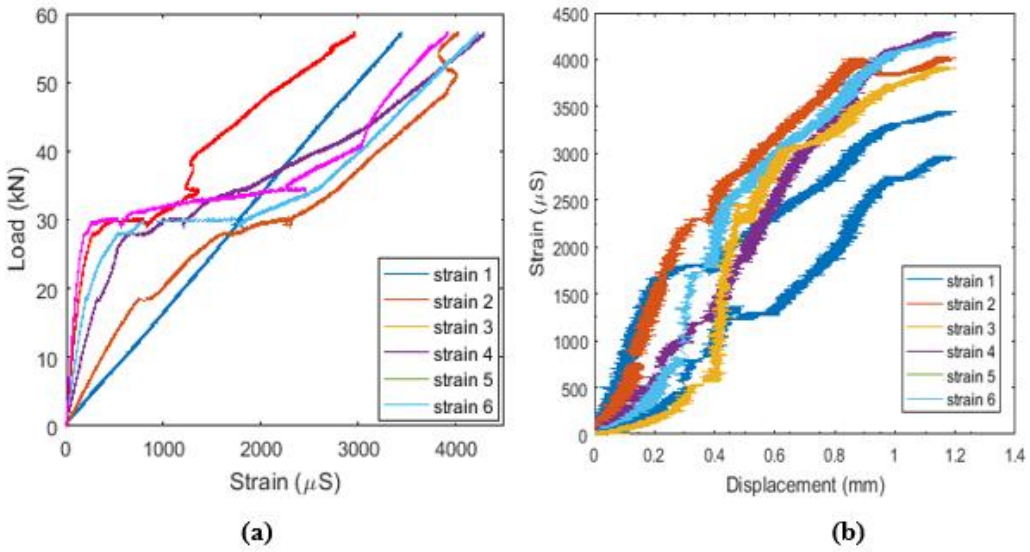

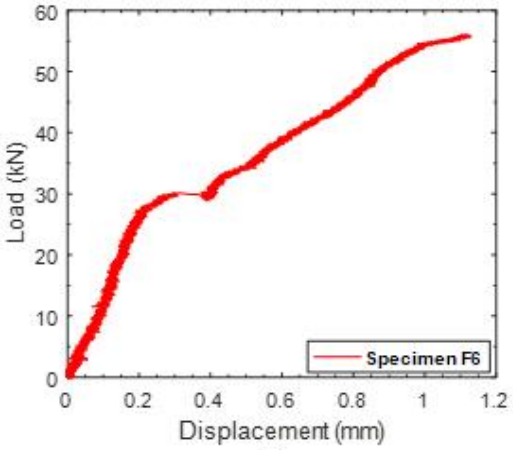

(c)

(d)

Fig. 3.4-14: *Specimen F6: (a) Load-Strain; (b) Strain-Displacement; (c) Load-Displacement; and (d) Failure Mode*

As the last specimen tested, ultimate load obtained was 57 kN. Below 30 kN, load-strain remains constant, however, above this load, linearity stops as seen from the five gauges [Fig. 3.4-14 (a)]. Gauge 1, which is attached on the unbonded region of the FRP, records linear load-strain all through.

Debonding starts at 30 kN. This is the load where micro-cracks begin to develop in concrete and progress into the bond area as witnessed with the other previously discussed specimens. From Fig. 3.4-14 (b), ultimate displacement is observed to be 1.15 mm.

Fig. 3.4-14 (d) shows failure mode for specimen F6 which appears mixed: concrete fracture and debonding. At the beginning of the specimen, damage is severe due to fracture failure from increased angular cracking. Severe debonding along the bond length is also witnessed.

3.5 SUMMARY OF EXPERIMENTAL WORK

This chapter, **Execution of Experimental Work**, was the focus of this study: evaluating how the bond strength between FRP and concrete is affected by the presence of transverse grooves in concrete. It detailed all the steps taken, from concrete and FRP preparation to the analysis of test results.

Following ASTM C192/ 192M-06 concrete preparation standards, 19 specimens were available for testing. Average compressive and tensile test values obtained were 34.50 MPa and 3.62 MPa respectively. Various surface preparations like grinding, cold water cleaning, and air pressure jet were performed prior to application of adhesive in order to ensure that the top weak concrete layer was removed. A special type of surface preparation named groove cutting was done with the purpose of understanding the bond behavior between FRP and concrete.

Waxing helped categorize specimens as either filled or unfilled. Filled specimens had grooves that were waxed on both sides of the bond area while unfilled specimens were filled all through the grooves. This process ensured that the epoxy was filled in the grooves (for F specimens) and that the epoxy was prevented from grooves (for U specimens). Prior to applying the adhesive epoxy, a primer epoxy was applied to all specimens which helped to eliminate any possible cavities and to seal porous aggregate.

Finally, prepared specimens were subjected to single shear pull out test after which the results summarized in Table 3.5-1 were obtained.

Table 3.5-1: *Summary Results of Tested Specimens*

Specimen	Max Load P_{max} (kN)	Ult Disp δ_{ult} (mm)	Failure Mode
***C1**	45	-	*FRP splitting*
***C2**	24	0.14	*FRP splitting*
***C3**	19	0.16	*FRP splitting*
C4	-	-	-
C5	32	0.66	*Debonding and Concrete Rupture*
U1	29	0.25	*Debonding*
U2	-	-	*Debonding*
U3	29	0.72	*Debonding and Concrete Rupture*
U4	30	0.89	*Debonding and Concrete Rupture*
U5	30	1.01	*Debonding and Concrete Rupture*
U6	38	0.24	*Debonding and Concrete Rupture*
F1	41	0.72	*Debonding and Concrete Rupture*
***F2**	57	-	*Debonding and Concrete Rupture*
F3	54	1.22	*Debonding*
F4	66	0.70	*Debonding and Concrete Rupture*
F5	65	0.88	*Debonding*
F6	57	1.57	*Debonding and Concrete Rupture*

* Specimens **NOT** used in the analysis and comparison

From Table 3.5-1, F specimens have higher load capacity compared to both U and C specimens. These specimens (F) have additional adhesive epoxy in the grooves that increases the bond contact area and as well as the acting as anchors. An additional load is required to overcome these extra contact areas and anchored regions in order to break the FRP off the concrete. Empty grooves, on the other hand, do not have much effect on the bond strength. U specimens support almost same amount of load as control specimens.

Average maximum load is 32.00 kN, 31.75 kN, and 56.60 kN for C, U, and F specimens respectively. Filled (F) specimens are 1.77 times stronger than control

specimens, which represents 77% percent increase in strength. Such increased strength is attributed to added epoxy adhesive in the grooves that provide extra bond areas. The filled grooves also act as an anchor system, delaying debonding. However, unfilled specimens are almost as strong as control specimens. With both filled and unfilled specimens having the same geometrical features, presence of additional epoxy in filled specimens plays a key role in increasing the composite strength between FRP and concrete.

After the test, two common failure modes were noted: debonding and concrete rupture. Debonding varied from mild to severe. Severe debonding left concrete specimens fully damaged along the bond length with some pieces of concrete chunks remaining on the FRP. Such failure signified quality bond between concrete and FRP. Areas with mild debonding had minimal concrete damage along the bond length. In this case, FRP did not have any concrete chunks left on it after failure. Such failure represented a bond region with limited surface preparation and/or poor application of the adhesive. On the other hand, cracks forming 45 ° angle with respect to the specimen surface originated from the pre-crack condition towards the front of the specimen. As loading increased, these cracks grew larger causing rupture failure that led to an angular concrete chunk breaking off from the rest of the concrete specimen. This phenomenon was also observed by other researchers like Mohammadi (2014).

All in all, it can be said that the presence of epoxy adhesive in concrete grooves improves concrete-FRP composite strength. As a special type of surface preparation, these grooves offer additional contact surface area and anchorage that need to be overcome during loading for FRP to break off the concrete substrate.

Chapter 4 Finite Element Modeling (FEM)

This chapter deals with numerical simulation of the three categories of specimens tested in the lab using Finite Element Modeling (FEM) software, ANSYS 17.1. It details both pre-processing steps like element selection, geometry set-up, and meshing as well as post-processing steps like non-linear solution generation of stress variation and cracking pattern. FEM results of stresses, cracking pattern and load-displacement curves are then compared to the experimental results obtained in the lab. Lastly, this chapter provides a summary of all the FEM work done.

4.2 ELEMENT SELECTION

SOLID 65

Element SOLID 65 was selected to model concrete in studying the bond behavior between concrete and FRP. This is a 3-D modeling element which can be modelled with or without rebar. In the current study, concrete is modelled without rebar and so, this element is appropriate. This element is capable of cracking in tension (in three orthogonal directions), crushing in compression, plastic deformation, and creep, which are typical behaviors for normal concrete.

The element has eight nodes with three degrees of freedom at each node: translation in the nodal x, y, and z directions as shown in Fig. 4.1-1 as well as isotropic

material properties. This element may also be assigned nonlinear material properties, which are important for the modelling concrete behavior accurately.

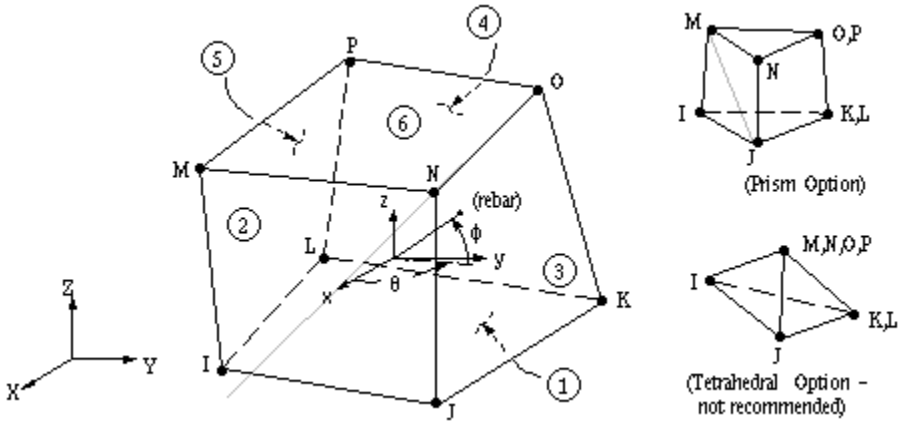

Fig. 4.1-1: *SOLID 65 Element Type (ANSYS 2016 Element Reference)*

Shear transfer coefficients for open and closed cracks; uniaxial tensile cracking stress; and uniaxial crushing stress were obtained and input into ANSYS as shown in Table 4.1-1. Typically, closed shear coefficient ranges from 0.00 – 1.00, where 0.00 represents a smooth crack which indicates complete loss of shear transfer while 1.00 represents a rough crack, whereby there is no loss of shear transfer. On the other hand, open shear transfer ranges from 0.20 – 0.50 (Razaghi et al, 2005). Following various trial-and-error method, open and closed shear transfer coefficients were selected as 0.20 and 0.10 respectively. Uniaxial cracking stress and uniaxial crushing stresses are taken as 3.6 MPa and 34 MPa respectively as obtained from the lab tests.

Table 4.1-1: *Non-Linear Input Properties for modeling SOLID65*

Property	Value
Temperature	0.00
Open Shear Trans Coefficient.	0.20
Closed Shear Trans Coefficient	0.10
Uniaxial Cracking Stress	3.60
Uniaxial Crushing Stress	34.0

Despite being an excellent candidate element for modelling concrete, element SOLID 65 has a few limitations and restrictions. All the elements must have eight nodes. As a nonlinear element, it requires iterative solution. Caution is required when both cracking and crushing are used together such that the load is applied slowly to avoid possible fictitious cracking of concrete before proper transfer can occur through closed crack (ANSYS, 2016)

SOLID 186

In the current study, SOLID 186 was used to model FRP, epoxy adhesive, and the steel plate attached to concrete. This is a higher order 3-D 20-node solid element which has quadratic displacement behavior. The element possesses three degrees of freedom per node: translation in the nodal x, y, and z directions. This element also supports plasticity, hyperelasticity, creep, stress stiffening, large deflection, and large strain capabilities. Despite having all these properties, in this research, this element is modeled as a linear elastic material.

SOLID 186 element exists in two forms: Homogeneous Structural Solid and Layered Structural Solid. Currently, the latter is considered since it can be used to model

both layered shells and solids. Fig 4.1-2 shows SOLID 186 Layered Structural Solid geometry. Anisotropic material properties can be input for this element, which corresponds to the layered coordinate directions that are based on the element coordinate system.

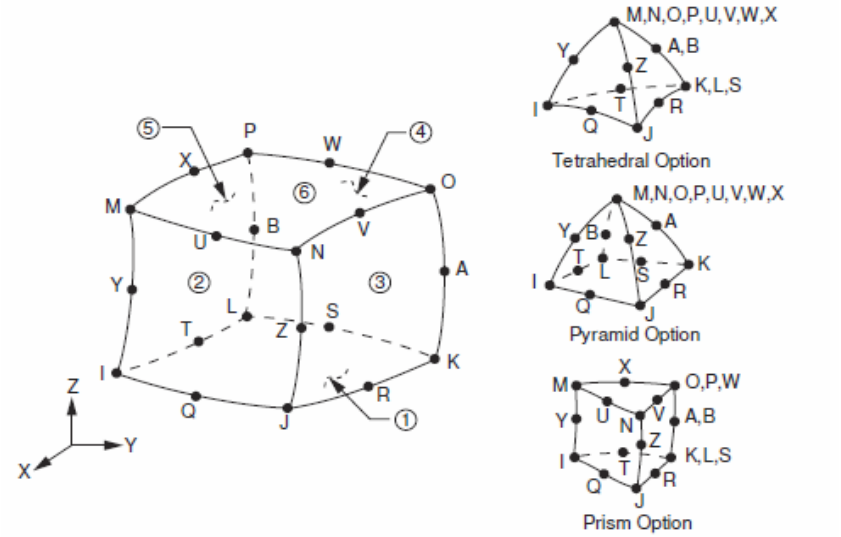

Fig. 4.1-2: *SOLID 186 Element Type (ANSYS 2016 Element Reference)*

4.2 MODELING

Material Properties

Concrete, FRP plate, epoxy adhesive, and steel plate were modeled with the material properties shown in Table 4.2-1. Both FRP and Epoxy material properties were provided by the manufacturer. Concrete properties were obtained by manipulating concrete compressive strength recorded in the lab. Lastly, steel properties were obtained from mechanics of material course materials.

Table 4.2-1: *Material properties*

Material	Elastic Modulus, E (GPa)	Poisson Ratio, v
Concrete	27.61	0.20
FRP	155	0.25
Epoxy	1.20	0.30
Steel Plate	200	0.30

Geometrical Setup

Once all the material properties (linear and nonlinear) were established, the next step involved setting up geometrical models for analysis in ANSYS 17.1. Three models were created: control model (C), unfilled model (U), and filled model (F). These models were created using the geometrical dimension obtained from the actual experimental setup.

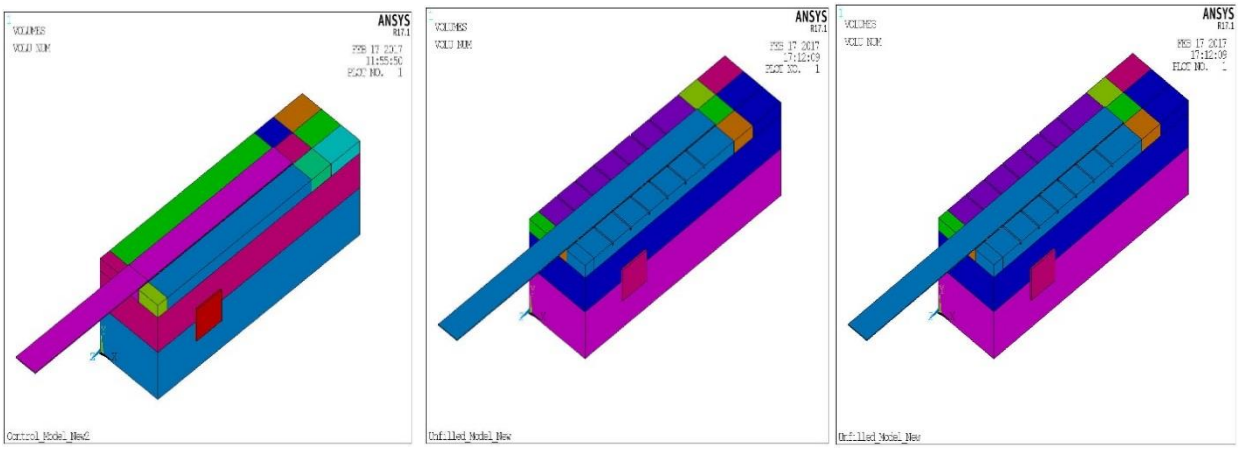

Fig. 4.2-1: *Geometrical setup for Control, Unfilled, and Filled models*

The next step was meshing the models and applying loads. Meshing was performed such that the FRP and the top 10 mm of concrete had finer meshing (using element edge length of 10 mm) in order to help improve the accuracy of the results at this location since it was where the debonding failure happened in the experimental test. The rest of concrete was meshed using element edge length of 50 mm i.e. coarse meshing.

Fig. 4.2-2 shows the meshed models. Note that convergence study was not conducted. All the meshes obtained were deemed sufficient since previous meshes that were tried exceeded the number of elements ANSYS software used could provide.

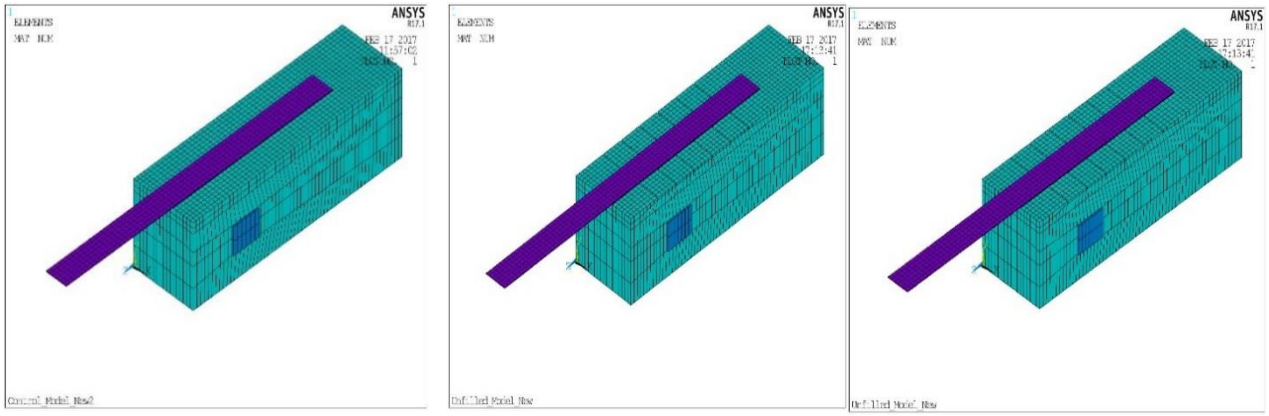

Fig. 4.2-2: *Meshed models*

The last step in the pre-processing step was applying the loads. Loads encompassed both actual loads and boundary conditions. To mimic the actual concrete blocks that were tested in the lab, the bottom face of all the models were fully constrained, i.e. all the degrees of freedom on those faces were set to zero (0). A half of the front face, from below, was constrained to eliminate any horizontal movement. Upward movement was restricted by adding constraint towards the end of the top face to mimic the clamping system that was used in the actual setup. Fig 4.2-3 shows areas constrained together with displacement control loading.

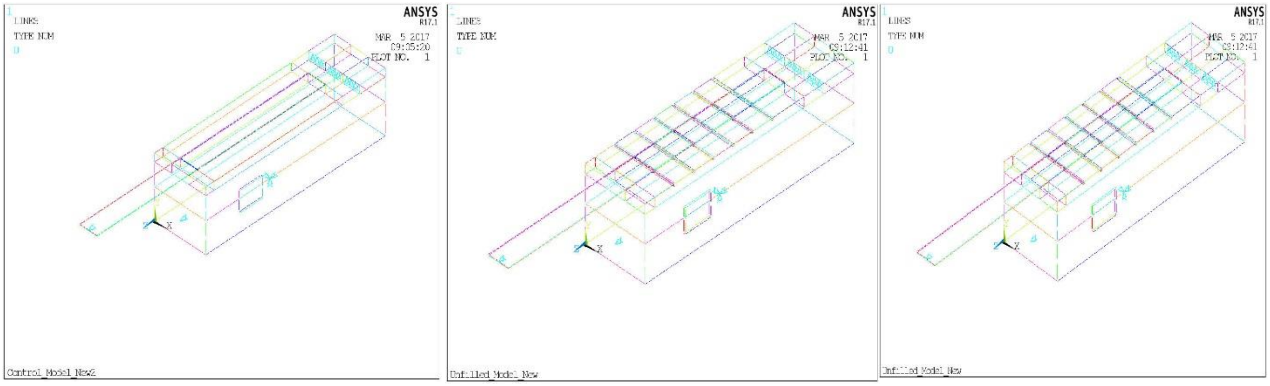

Fig. 4.2-3: *Load Application – boundary condition and displacement control*

Finally, the load was applied on the front face of the FRP. Load, applied as displacement, was broken down into steps which were further divided into sub-steps to improve the accuracy of the nonlinear solution. Four steps with 0.3 mm increments were input for control model; five steps with 0.3 mm increments for unfilled; and nine steps with 0.3 mm increments for filled model. In addition, convergence criteria on displacement control was performed such that tolerance was kept as default (0.001) while minimum reference was input as 0.001.

4.3 RESULTS AND COMPARISON

Stress Variation

Stress in the direction of load application was checked in the three models to ascertain how it varied from one material to another. As predicted, the FRP was largely under tensile stress (since it was being pulled on) while concrete was largely under compression from the direction of applied load i.e. z-direction. Maximum tensile stress

was observed to occur in FRP near the pre-crack condition. Fig. 4.3-1 shows nodal stress variation in the three models. After running each model, it was observed that both control and unfilled models supported 35 kN compared to the 32 kN recorded in the lab while filled model supported 65 kN compared to the 56 kN recorded in the lab. This then indicates presence of high tensile stress in FRP in filled model than that observed in unfilled and control as indicated in Fig. 4.3-1. High stresses observed on FRP in the filled model indicate the presence of filled grooves which act as anchors, something that was also observed in the experimental results. Stress pattern for control and unfilled models appear similar compared to filled pattern. This suggests that empty grooves hardly affect the bond strength.

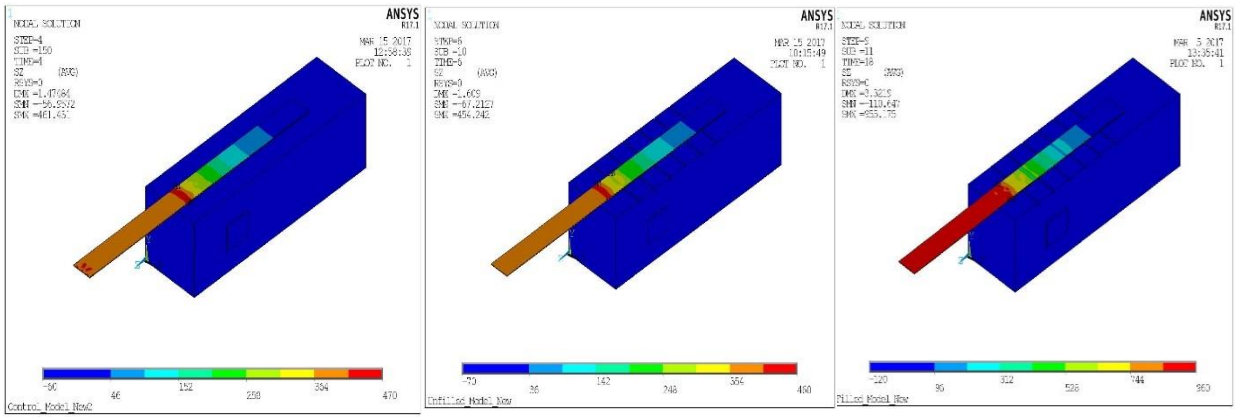

(a) **(b)** **(c)**

Fig. 4.3-1: *Nodal stress (MPa) variation in the z-direction for Control (a), Unfilled (b), and Filled (c) models along the direction of load application*

Cracking Behavior

To simulate cracking behavior that was observed in the lab, non-linear concrete properties shown in Table 4.4-2 were input in ANSYS. After analysis, cracking pattern was obtained and compared to the experimental shown in Fig. 4.3-2 (a) – (c). It is observed that the cracking patterns for the three models mimics those obtained in the lab. Cracking pattern observed on specimen C5 (Fig.4.3-2a) mimics that observed using FEM in which there is major damage at the beginning of the bond length.

Similarly, cracking pattern in Fig. 4.3-2 (b) mimics that of specimen U5 in which damage (cracks) dominate the first two grooves then slowly decrease to the other end of the bond length. Cracking pattern on the filled model also mimics the actual specimen that was tested in the lab. When compared to the other two models, it is seen that filled model shows more cracking, indicating higher degree of stress in its bond interface. This is alluded to the additional epoxy in the grooves that help delay cracking up to higher loads. Note that first stage cracks are indicated by the red color, second stage by green, and final stage cracks by blue color as seen in Fig. 4.3-2.

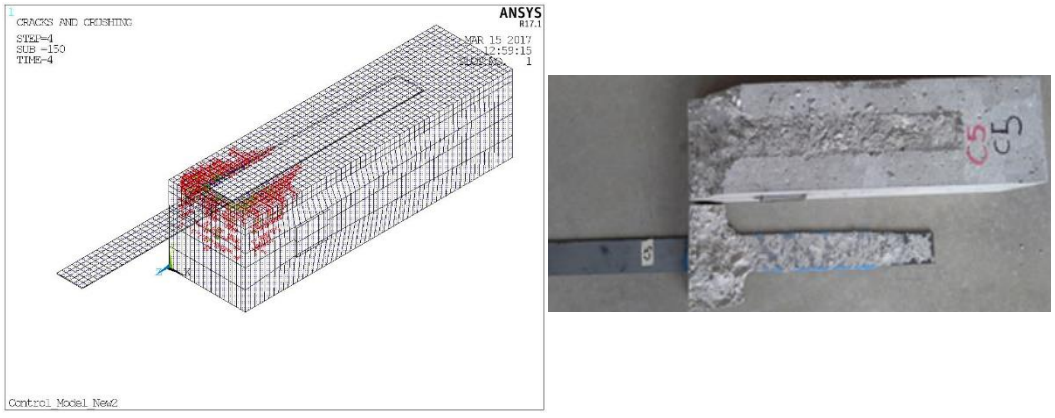

Fig. 4.3-2 (a): *Crack pattern comparison for control specimen*

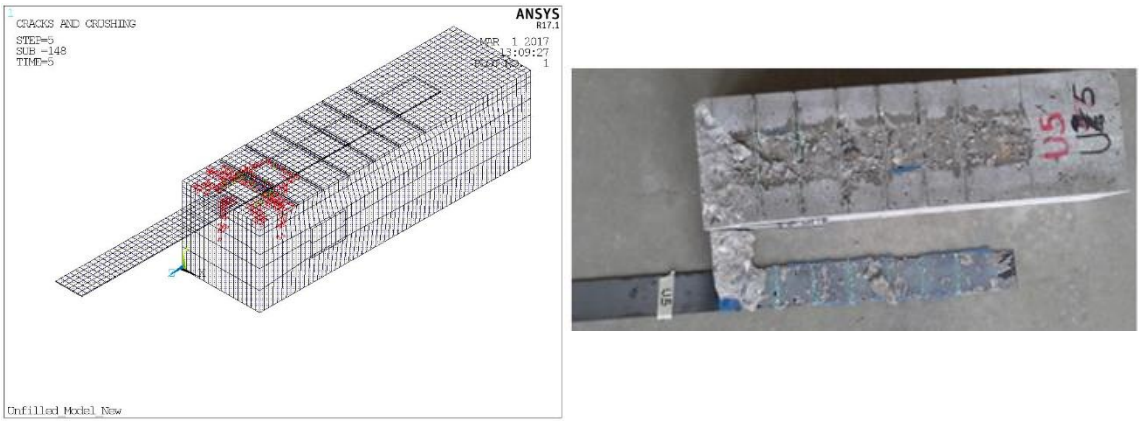

Fig. 4.3-2 (b): *Crack pattern comparison for unfilled specimen*

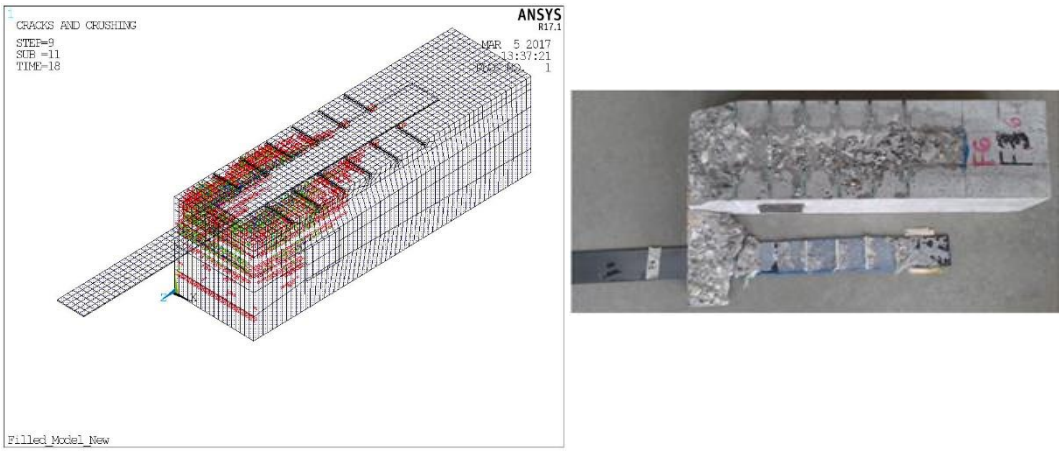

Fig. 4.3-2 (c): *Crack pattern comparison for filled specimen*

Load – Displacement Curves

Fig. 4.3-3 (a) – (c) shows load-displacement comparison between experimental and numerical (FEM) results for control, unfilled, and filled specimens. Displacement is obtained by picking a node that is located 25 mm from the edge of concrete i.e. on the edge of the pre-crack condition. This node is selected since it is where the LDS was

placed in the actual experimental set up. Note that several nodes at this location had same displacement and so, picking a single node was sufficient.

On the other hand, load was obtained from the front edge of the FRP. Since there was minimal stress variation on this edge, a single node was selected. The two parameters, stress and displacement, were then imported into an excel file where the stress was converted into load by multiplying the stress with cross-section area (1.5 mm x 51 mm). Load and displacement were then plotted as seen from Fig. 4.3-3 (a) – (c).

The three plots have overall linear relations although there are a few points of load dropping and changing of slopes. Increasing both uniaxial cracking and crushing shear coefficient appeared to increase the linearity without generating the softening part. With the two coefficients having been input into ANSYS based on a trial-and error-method, it is suspected that lack of proper combination of the two could be the cause of missing softening part on the graphs. Although the softening part is not observed however, there are few changes of slope along the three FEM graphs, indicating cracking that is observed in Fig. 4.3-3 (a) – (c).

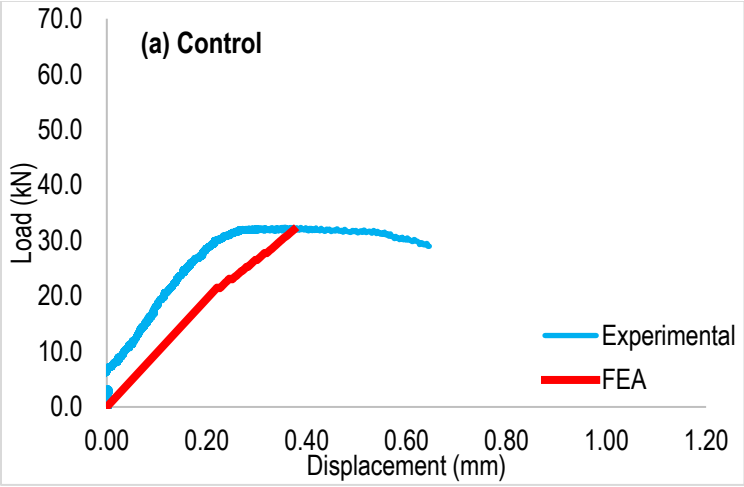

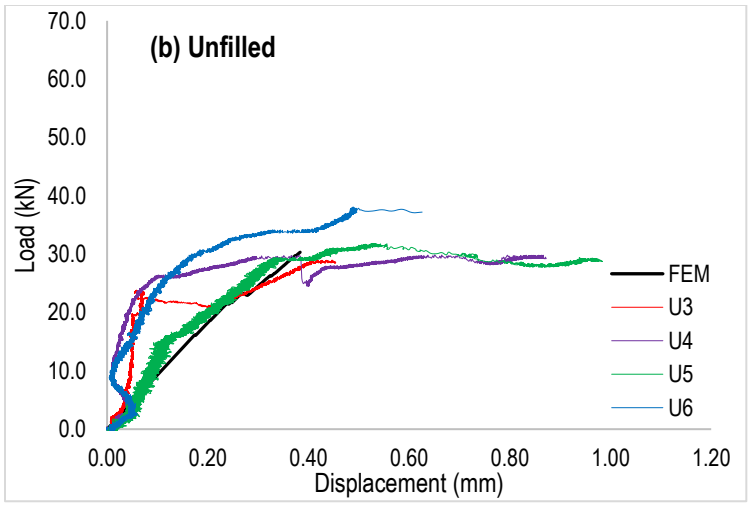

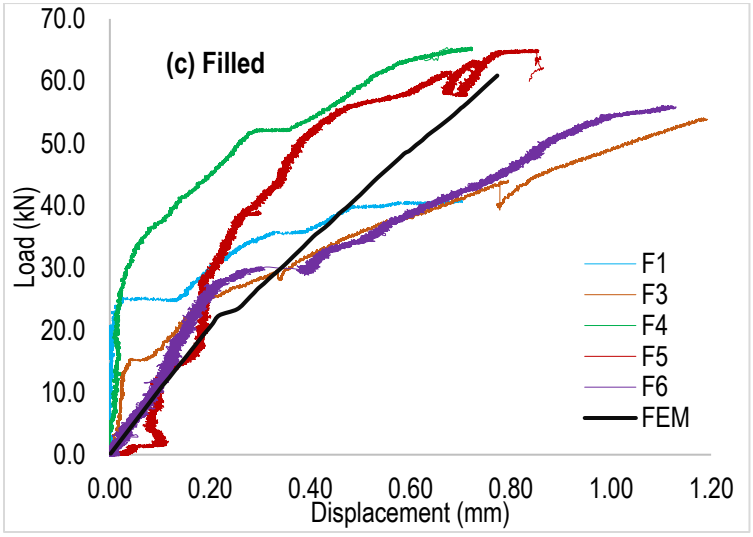

Fig. 4.3-3: *Load-displacement for control (a), unfilled (b), and filled (c) specimen*

4.4 SUMMARY OF FEM

This chapter dealt with numerical analysis of the three categories of the specimens that were tested in the lab. Results obtained were then compared to the experimental results. Element SOLID 65 was selected to model concrete while SOLID 186 was selected to model FRP, epoxy and steel plate.

Geometrical modeling was done following physical dimensions obtained from the lab. This was part of the pre-processing step which also entailed inputting nonlinear properties for concrete as well as displacement convergence criteria. Lastly loads were applied as displacement control.

In post-processor, nodal stress, concrete cracking, and load-displacement were checked. As expected, much of the FRP plate was in tension while the concrete was largely compression in the direction of load application (z-direction). Cracking pattern of the concrete obtained in all the three categories, mimicked the actual cracks observed on the actual specimens. Cracks decreased from the edge of the concrete along the bond length. The load-displacement obtained for the three specimens did not mimic the ones obtained from the lab. Only the linear region of the curve was obtained, however the softening part of the curve was not. This is believed to have been caused by an imbalance between uniaxial shear crack and crush coefficients. Additionally, insufficient convergence criteria based on the available concrete properties was also suspected to be the cause.

Chapter 5 Conclusions and Future Work

5.1 CONCLUSIONS

The current study was aimed at evaluating how the presence of grooves on different CFRP-concrete specimens affected the bond behavior. The following paragraphs highlight major takeaways from the study.

Flexural capacity of any deteriorated concrete member can be greatly improved by attaching CFRP material on the tensile face of the member using adhesive epoxy. This then increases the lifespan of the rehabilitated structure. Surface preparation is perhaps the most critical process which affects the bond behavior between concrete and CFRP. By scrapping off the top weak layer of concrete, a strong surface is exposed which can absorb and hold epoxy that binds FRP to concrete. The bond behavior between concrete and FRP was studied further by introducing a special type of surface preparation known as *grooving*. From the study, it was found that empty grooves did not affect the bond strength between FRP and concrete. Tests results revealed that specimens with empty grooves are as strong as the control specimens. However, when these grooves are filled with adhesive epoxy, bond strength increases by 77%. The presence of adhesive in the grooves act as anchors, delaying debonding of FRP thus increasing load capacity. These grooves also provide an additional bond contact area that must be overcome before FRP failure.

Similarly, numerical analysis using ANSYS 17.1 supported the results obtained from the lab. Filled specimen supported much load compared to the both control and unfilled specimens. Cracking patterns obtained from FEM were also like those observed in the lab whereby the cracks decreased along the bond length from the edge of the specimens.

5.2 FUTURE WORK

Even though the goal of this study has been achieved, however, few improvements on some of the methods and approaches used could help improve the results and minimize some of the errors witnessed during the tests. The following recommendations are suggested.

In running the same tests, instead of attaching the LDS on the small steel angle attached on the FRP, the two can be glued together to minimize the motion and vibrations of the LDS since it is a sensitive equipment. This would also ensure that the LDS does not slide off the plate during the tests; something that is suspected to have affected some of the results. Concrete alignment with the actuator is also believed to have been the cause of erroneous behavior observed in some load-displacement graphs. This could be minimized by first lightly tightening the concrete specimen and then applying the load. Once the erroneous behavior has been surpassed, the system can be the concrete can then be tightened down before the actual loading.

While the current study also introduced Finite Element Modeling (FEM) of the three types of specimens tested in the lab, however, it does not fully explore the analysis. Therefore, with experimental results already available, a thorough non-linear analysis of the specimens using FEM to determine load-displacement as well as stress variation particularly in the grooved regions would improve the understanding the bond behavior between FRP and concrete. To add on, groove spacing and depth could be parameters for the FEM analysis in future.

In the current study transverse grooves have shown to be effective in providing additional strengthen to the concrete-FRP composite by delaying debonding. However, for practical FRP-concrete beam applications, such grooves could be a source of angular shear cracks. Its actual effects on shear cracking in reinforced concrete beams should be studied in future.

REFERENCES

[1] ACI Committee 440. (2008). "Guide for the Design and Construction of Externally Bonded FRP Systems for Strengthening Concrete Structures." *ACI 440.2R-08*

[2] Aram R.M., Czaderski D., and Motavalli M. (2007). "Debonding Failure Modes of Flexural FRP-Strengthened RC Beams." *Composites Part B: Engineering 39 (2008) 826-841*

[3] ASTM International. (2006). "Standard Practice for Making and Curing Concrete Test Specimens in the Laboratory." *Designation: C 192/C 192M – 06*

[4] ASTM International. (2000). "Standard Test Method for Tensile Properties of Polymer Matrix Composite Materials." *Designation: D 3039/D 3039M – 00*

[5] Bizindavyi L. and W. Neale (1999). "Transfer Lengths and Bond Strengths for Composites Bonded to Concrete." *Journal of Composites for Construction. November 1999, 3(4):* pp 153-160.

[6] B. Wan, Sutton, M.F., Petrou, K.A. Harries, N. Li (2006). "Investigation of bond between fiber reinforced polymer and concrete undergoing global mixed mode I/II loading" *ASCE Journal of Engineering Mechanics*, 130 (12) (2004), pp. 1467–1475

[7] Caggiano A., Martinelli E., and Etse G.J. (2011). "Bond Behavior of FRP Strips Glued on Concrete: A Novel Zero-Thickness Interface Model." *Asociacion Argentina de Macanica Computacional*. Vol. XXX, pp. 1779-1788.

[8] Ceroni F. and Pecce M. (2010). "Evaluation of Bond Strength in Concrete Elements Externally Reinforced with CFRP Sheets and Anchoring Devices." *Journal of Composites for Constructions. Sept-Oct. 2010*. DOI: 10.1061/_ASCE_CC.1943-5614.0000118

[9] Chen J.F. and Teng J.G. (2001). "Anchorage Strength Models for FRP and Steel Plates bonded to Concrete." *Journal of Structural Engineering, (2001), 127(7): 784-791*.

[10] Chu I.Y., Woo K.S., and Lee Y. (2015). "Experimental Study on Interfacial Behavior of CFRP-Bonded Concrete*." KEPCO Journal on Electric Power and Energy, VOL. 1 No.1 September 2015.* ISSN 2465-8111 DOI http://dx.doi.org/10.18770/KEPCO.2015.01.01.127

[11] Dong Y., Zhao M., and Ansari F. "Failure Characteristics of Reinforced Concrete Beams Repaired with CFRP Composites."

[12] Jayalin. D, Prince Arulraj. G, and Karthika. V. (2015).” Analysis of Composites using ANSYS.” *IJRET: International Journal of Research in Engineering and Technology*. Volume: 04. Special Issue: 09. *eISSN:2319-1163. pISSN: 2321-7308.*

[13] Kotynia R. (2005). “Debonding Failures of RC Beams Strengthened with Externally Bonded Strips.” *Preceedings of the International Symposium on Bond Behavior of FRP in Structures (BBFS 2005) Cheng and Teng (ed). 2005 International Institute for FRP in Construction*

[14] Lee Y.J., Boothby T.E., Bakis C.E., and Nanni A. (1999). “Slip Modulus of FRP Sheets Bonded to Concrete.” *Journal of Composite Construction, 1999, 3(4).* Vol. 3, No. 4, November 1999., pp 161-167.

[15] Lu X.Z., Teng J.G., Ye L.P., and Jiang J.J. (2005). “Bond-Slip Models for FRP Sheets/Plates bonded to Concrete.” *Engineering Structures 27 (2005) 920-937*

[16] Mazzotti. C, Savoia. M, and Ferracuti B. (2007). " An experimental study on delamination of FRP plates bonded to concrete.” *Construction and Building Materials 22 (2008) 1409-1421*

[17] Mohammadi T. (2014). “Failure Mechanics and Key Parameters of FRP Debonding from Cracked Concrete Beams”. Dissertation Thesis: Marquette University. Chaps. 1-5

[18] Mostofinejad, D. and Mahmoudabadi, E. (2010). “Grooving as Alternative Method of Surface Preparation to Postpone Debonding of FRP Laminates in Concrete Beams*.” J. Compos. Constr., 2010, 14(6): 804-811*. DOI: 10.1061/_ASCE_CC.1943-5614.0000117

[19] Mostofinejad, D. and Hosseini, A. (2013). “Effect of groove characteristics on CFRP-to-concrete bond bevior of EBROG joints: Experimental study using particle image velocimetry (PIV*).” Construction and Building Materials 49 (2013) 364–373*

[20] Mostofinejad, D. and Hosseini, A. (2013). “Experimental investigation into bond behavior of CFRP sheets attached to concrete using EBR and EBROG techniques*.” Composites: Part B 51 (2013) 130–139*

[21] Nakaba K., Kanakubo T., Furuta T., and Yoshizawa H. (2001). “Bond Behavior between Friber-Reinforced Polymer Laminates and Concrete.” *ACI Structural Journal*. Volume 98, No. 3, May-June 2001. Title No. 98-S34

[22] Obaidat T. Y. (2013). “Effects of Interfacial Properties on the Bond behavior of Retrofitted Members.” *Jordan Journal of Civil Engineering, Volume 7, No. 2, 2013*

[23] Ozbakkaloglu T. and Saatcioglu M. (2009). "Tensile Behavior of FRP Anchors in Concrete." *Journal of Composite for Constructions. March-April 2009, 13(2).* pp 82-92. DOI: 10.1061/(ASCE)1090-0268(2009)13:2(82)

[24] Pan J. and Leung K.Y.C. (2006). "Debonding along the FRP-Concrete Interface under combined Pulling/Peeling Effects." *Engineering Fracture Mechanics 74 (2007) 132-150*

[25] Pellegrino C. and Modena C. (2008). "Bond-Slip Relationship between FRP Sheets and Concrete." *Fourth International Conference on FRP Composites in Civil Engineering (CICE2008).* 22-24 July 2008, Zurich, Switzerland.

[26] Pham B. H. and Al-Mahaidi R. (2007). "Modelling of CFRP-Concrete Shear-Lap Tests." *Construction and Building Materials 21 (2007).* pp 727- 735

[27] Razaghi, A. J, Hosseini, F. Hatami, "Finite element method application in nonlinear analysis of reinforced concrete structures." *Second Nat Congr Civil Eng* (2005)

[28] Swamy R.N. and Mukhopadhyaya P. (1999). "Debonding of Carbon-Fiber-Reinforced Polymer Plate from Concrete Beams." *Proc. Instn Civ. Engrs Structs & Bldgs, 1999, 134 Nov., 301-317. Paper 11961*

[29] Teng J.G. and Chen J.F. (2007). "Debonding Failures of RC Beams Strengthened with Externally Bonded Reinforcement: Behavior and Modelling." *Asia-Pacific Conference on FRP in Structures (APFIS 2007). S.T. Smith (ed). 2007 International Institute for FRP in Construction*

[30] Teng J.G., Lam L., Chen J.F., Dai J.G., and Yu T (2009). "FRP Composites in Structures: Some Recent Research." *The Second Official International Conference of International Institute for FRP in Construction for Asia-Pacific Region.*

[31] Teng J.G., Zhang J.W., and Smith S.T. (2002). "Interfacial Stresses in Reinforced Concrete Beams Bonded with a Soffit Plate: A Finite Element Study." *Construction and Building Materials 16 (2002).* pp 1-14

[32] Toutanji H. and Ortiz G. (2001). "The Effects of Surface Preparation on the Bond Interface between FRP Sheets and Concrete members." *Composite Structures 53 (2001) 457-462.*

[33] Yao J., Teng J.G., and Chen J.F (2005). "Experimental Study on FRP-to-Concrete Bonded Joints." *Composites Part B: Engineering 36 (2005) 99-113*